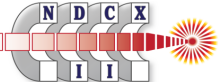
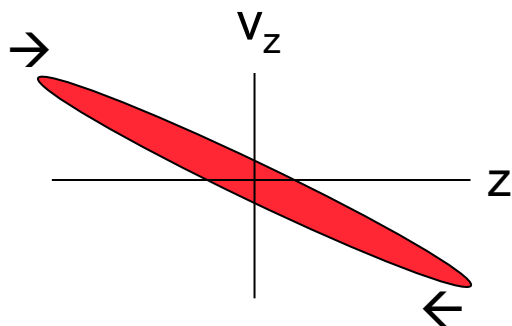


Extras

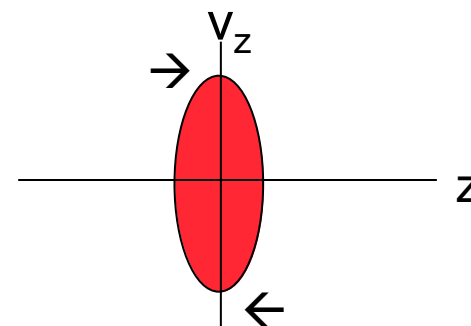


The “drift compression” process is used to shorten an ion bunch

- Induction cells impart a head-to-tail velocity gradient (“tilt”) to the beam
- The beam shortens as it moves down the beam line (pictures in beam frame):



Initial beam,
with velocity tilt

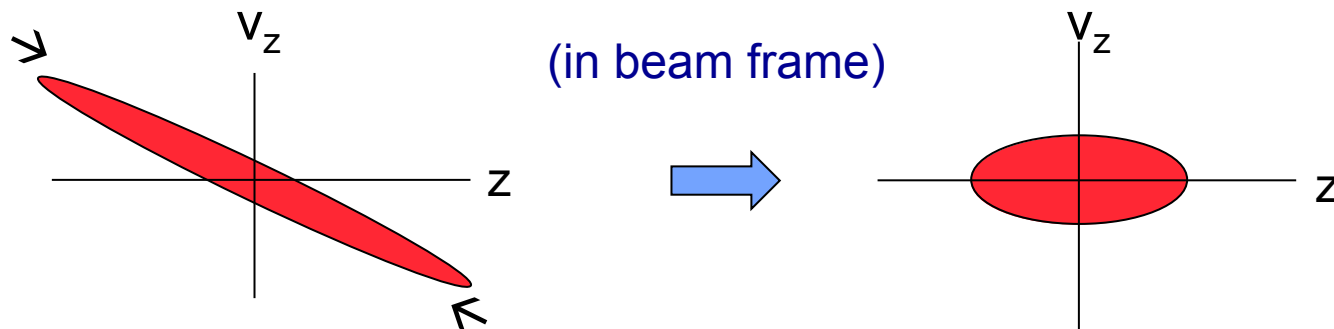


compressed beam

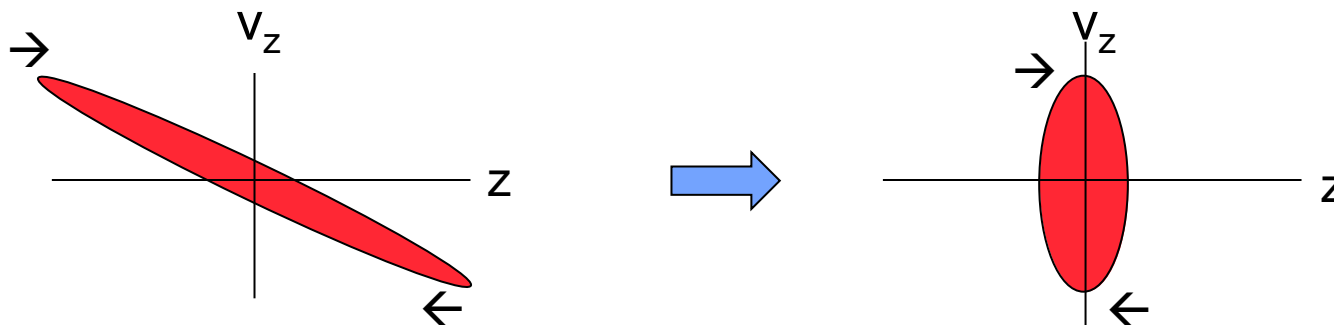
- Space charge, if present, limits this inward motion
- To obtain a short pulse on target, we introduce neutralizing plasma; this is **neutralized drift compression**.

The “drift compression” process is used to shorten an ion bunch

- Induction cells impart a head-to-tail velocity gradient (“tilt”) to the beam
 - The beam shortens as it “drifts” down the beam line
-
- In **non-neutral drift compression**, the space charge force opposes (“stagnates”) the inward flow, leading to a nearly mono-energetic compressed pulse:

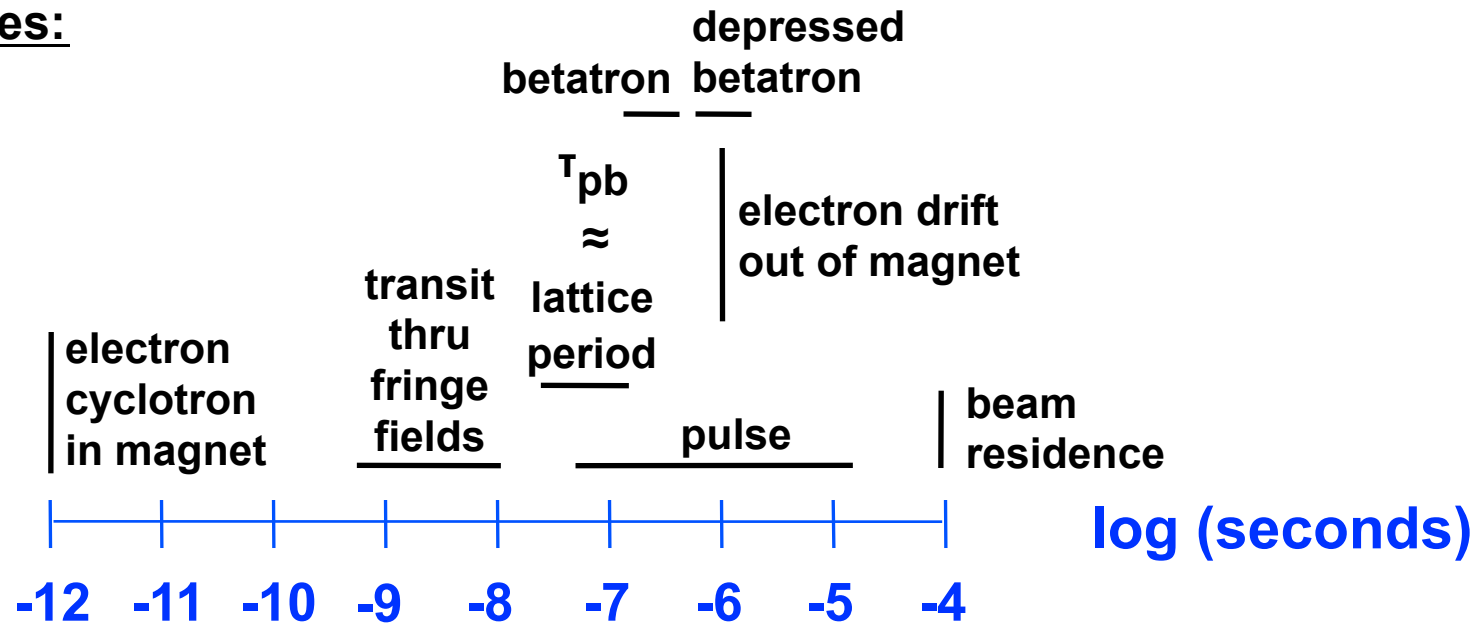


-
- In **neutralized drift compression**, the space charge force is eliminated, resulting in a shorter pulse but a larger velocity spread:

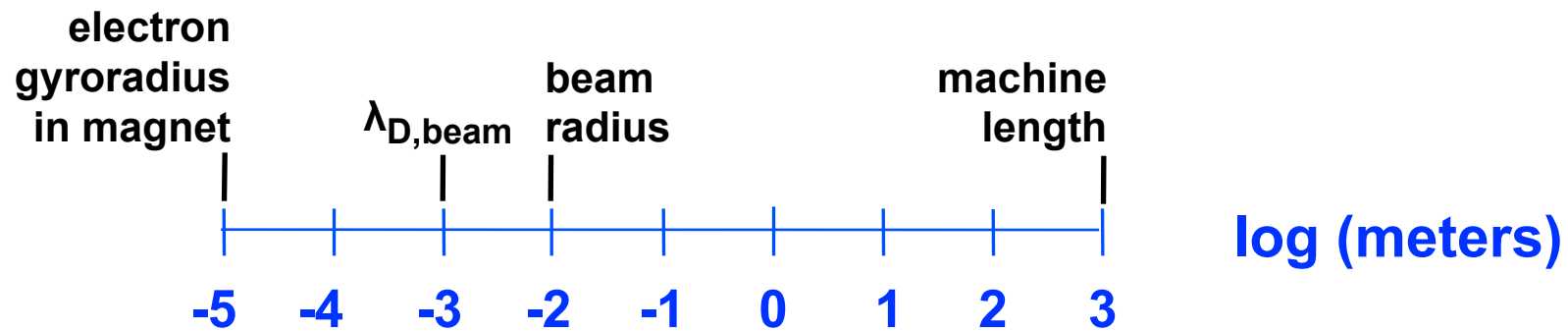


For HIF driver, time and length scales span a wide range

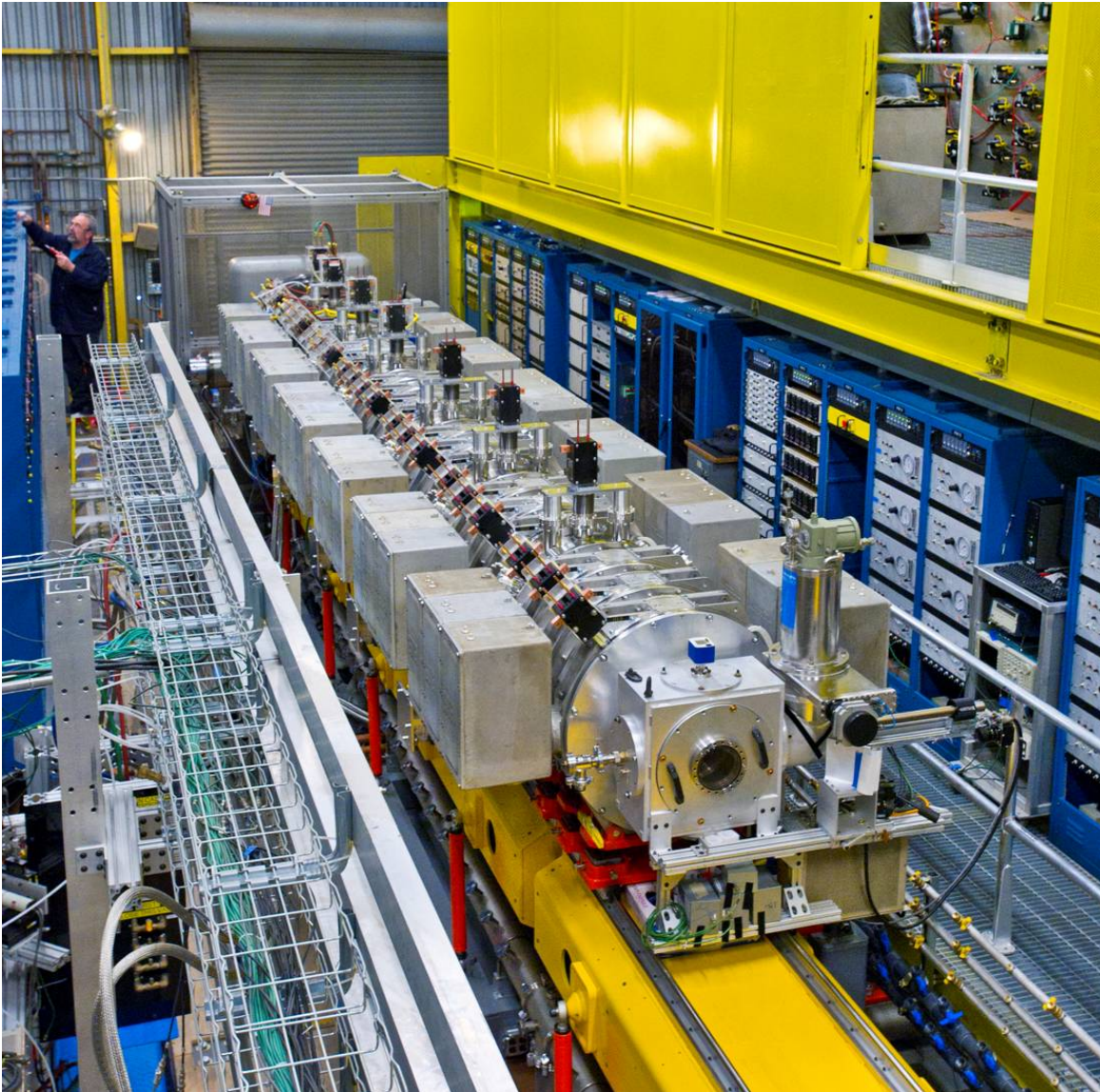
Time scales:



Length scales:

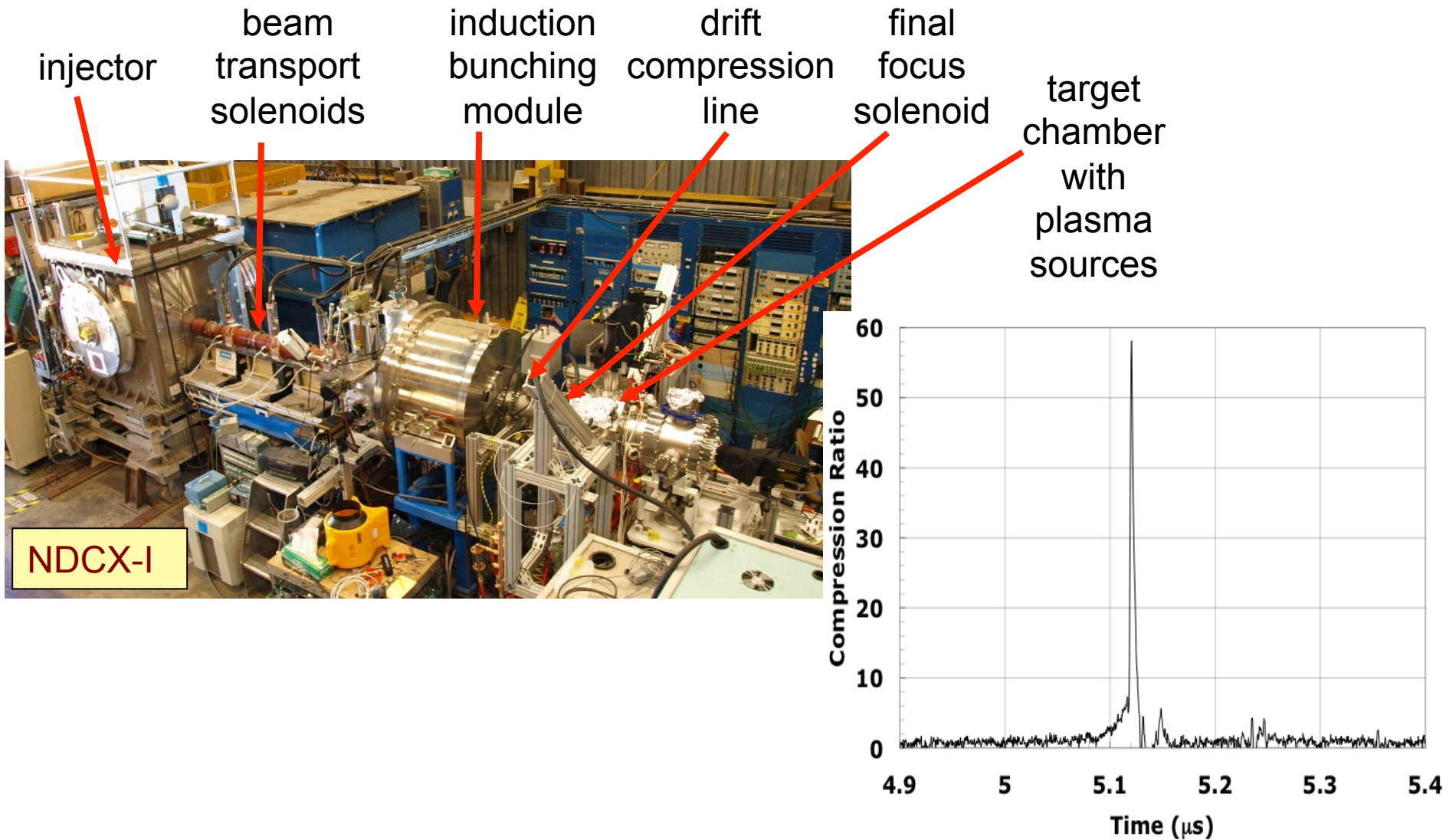


NDCX-II at LBNL



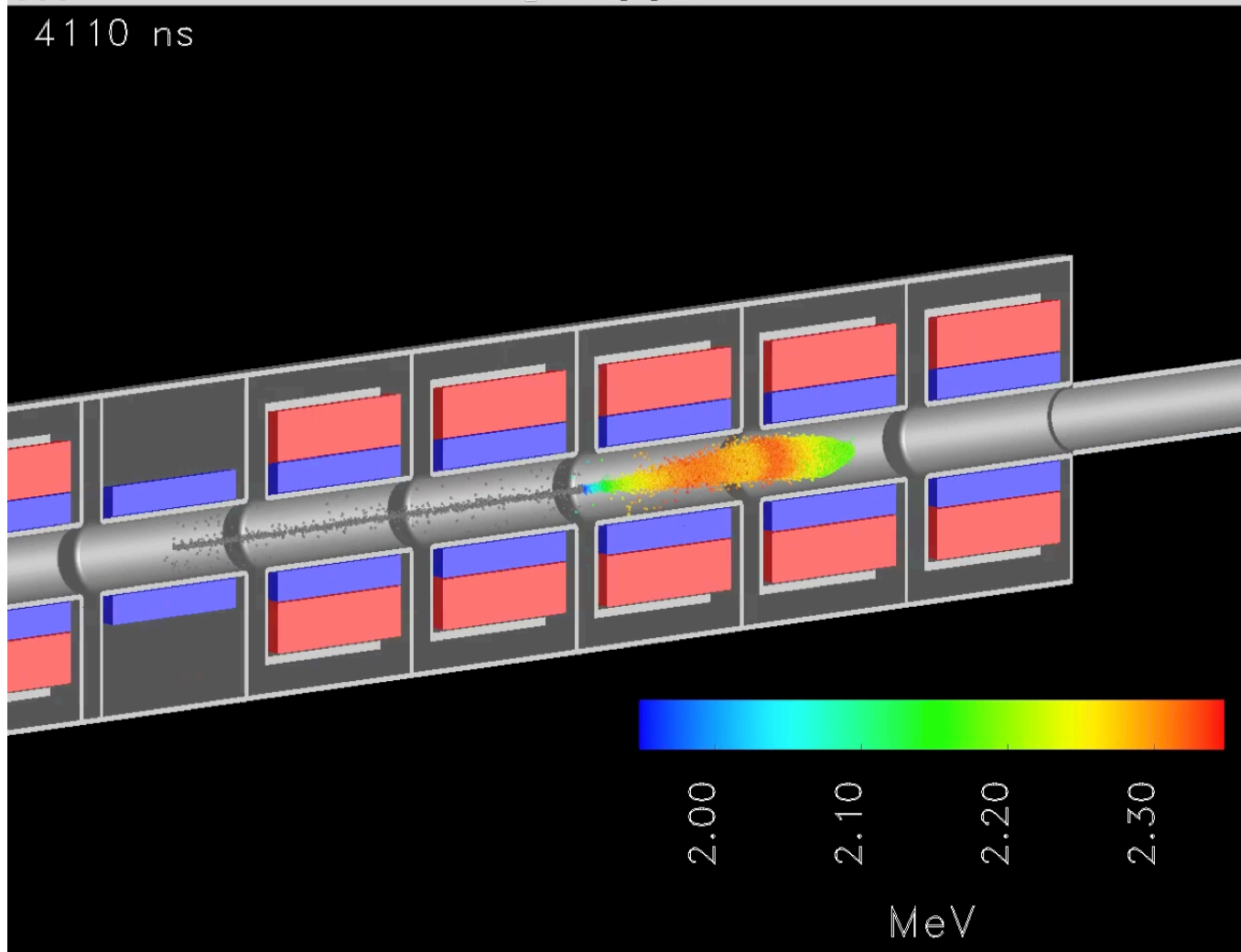
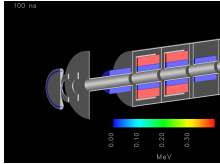
- FES approved the project early in 2009.
- Construction began in July 2009.
- Construction is now complete.
- Commissioning is partially complete: 7 of the 12 accelerating cells have been connected to high-voltage supplies
- Beneficial operation has begun, using the initial beam for materials-defect studies

Neutralized Drift Compression Exp't (NDCX-I) at LBNL routinely achieved current and power amplifications exceeding 50x



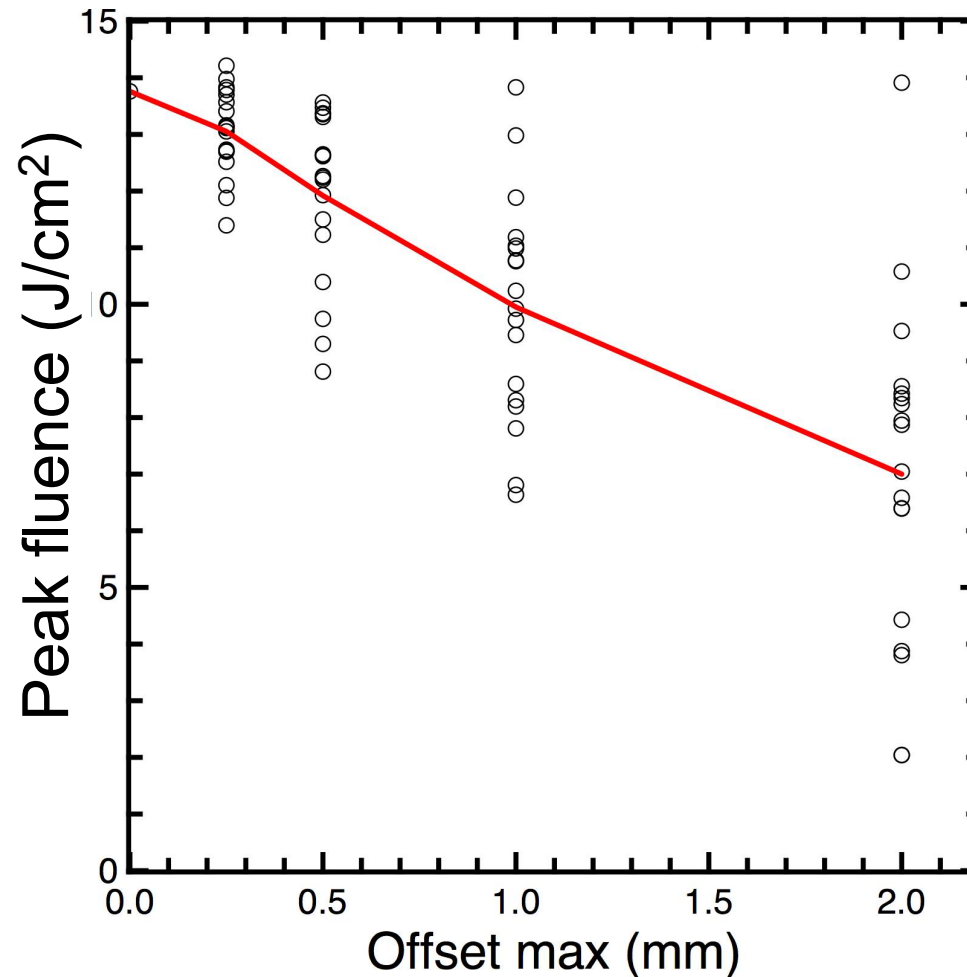
Video: Warp 3D simulation of 18-cell NDCX-II, including random offsets of solenoid ends by up to 2 mm (0.5 mm is nominal)

play video



Warp 3D simulations indicate slow degradation of the focus as misalignment of the solenoids increases (without steering)

- Random offsets in x and y were imposed on the solenoid ends.
- The offsets were chosen from a uniform distribution with a set maximum.

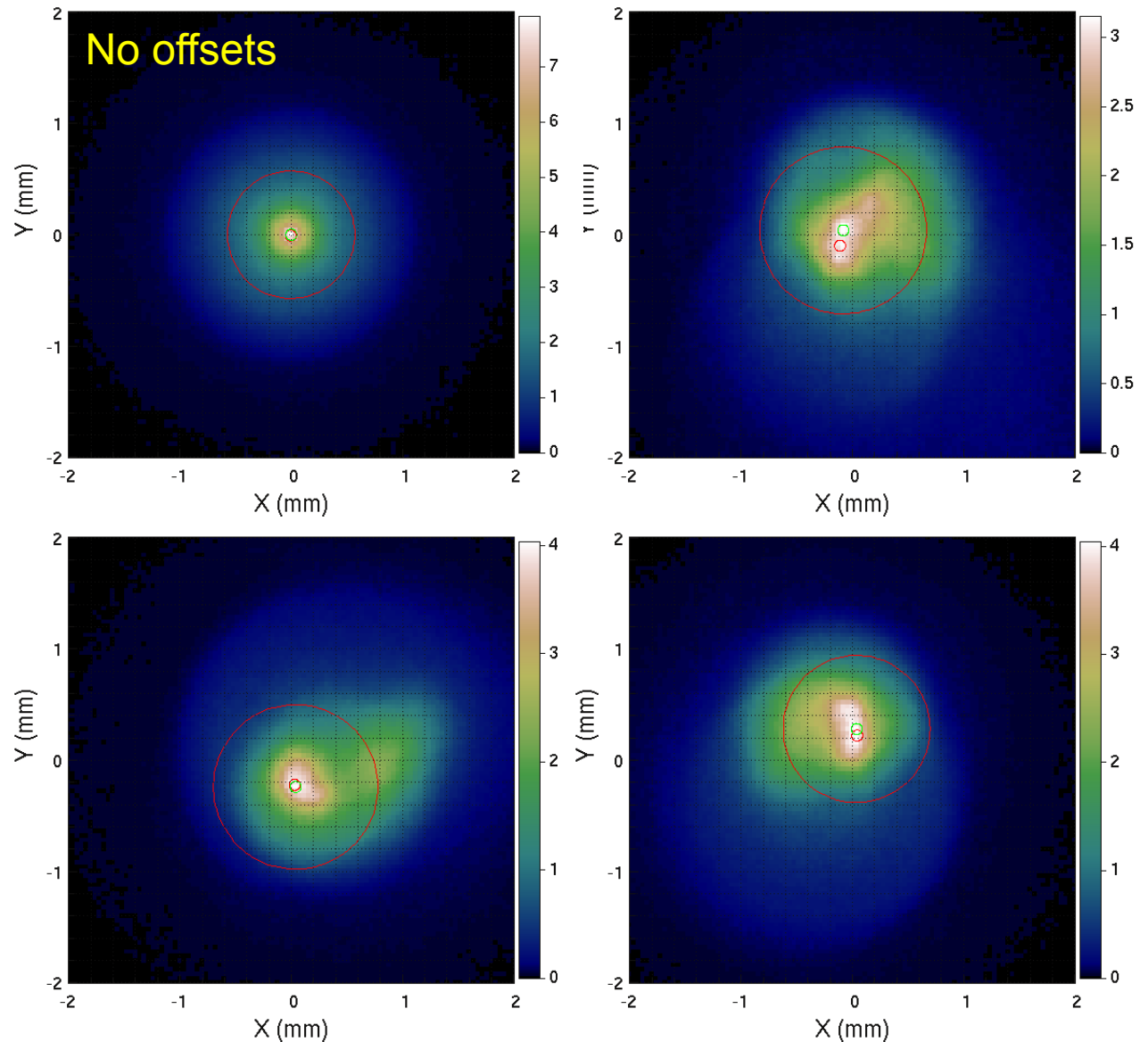


(This series used an older 15-cell design based on a 2 mA/cm² source)

35g-15

Example deposition patterns on target (study of misalignments)

- The beam deposition patterns for three different realizations of the solenoid offsets, with 0.5 mm max offset
- These give an idea of what distortions might be seen
- Red circle includes half the deposited energy
- Smaller circles, with 0.1 mm diameter, are at hot spots



Simulations were essential to the development of the NDCX-II physics design

- New, fast 1-D (longitudinal) discrete-particle code ASP enabled finding an attractive operating point within the large parameter space

It was essential to combine judgment and automatic optimization

- Injector, transverse beam confinement, and final focusing were developed using the discrete-particle code Warp in (r,z) geometry
- A centroid-offset model in ASP enabled us to establish the spacing of beam position monitors and “steering” dipole magnets
- We used 3-D Warp calculations to assess performance in the presence of imperfections, set tolerances

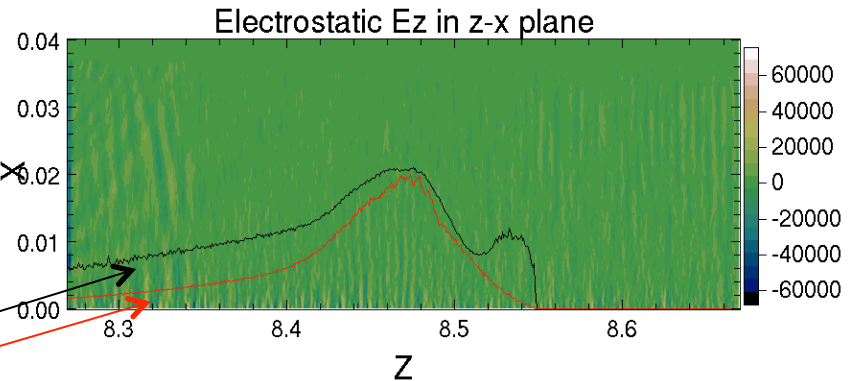
Plasma structures form in beam

Example with FEPS $N_p = 10^{16} / m^3 \sim N_b$

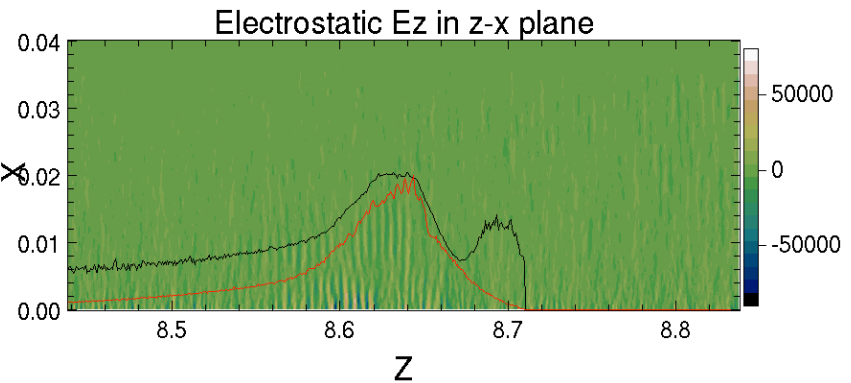
$t = 3.94 \mu s$

Black – beam envelope

Red ~ beam current



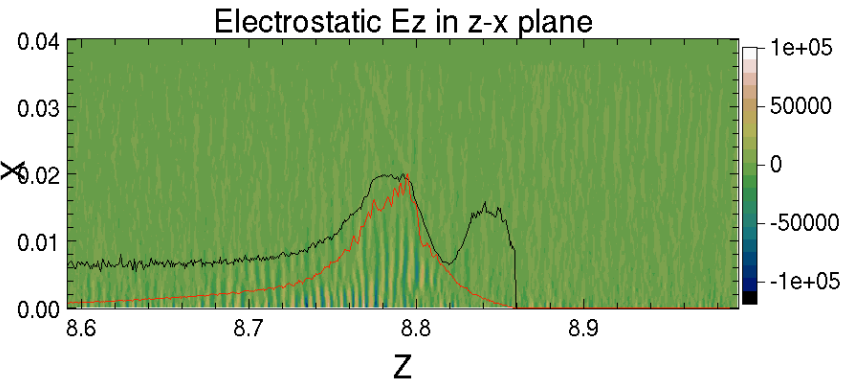
$t = 3.97 \mu s$



Wavelength depends on density

- close to unstable e-i two-stream mode
- > plasma oscillation, ~ 1mm

$t = 3.99 \mu s$



1-D PIC code ASP (“Acceleration Schedule Program”)

- Follows (z, v_z) phase space using a few hundred particles (“slices”)
- Accumulates line charge density $\lambda(z)$ on a grid via particle-in-cell
- Space-charge field via Poisson equation with finite-radius correction term

$$\frac{\partial^2 \phi(z)}{\partial z^2} - k_{\perp}^2 \phi(z) = -\frac{\lambda(z)}{\epsilon_0 \pi r_{\text{beam}}^2} ; \quad E_z(z) = -\frac{\partial \phi(z)}{\partial z}$$

$$k_{\perp}^2 = \frac{4}{g_0 r_{\text{beam}}^2} ; \quad g_0 = 2 \ln \frac{r_{\text{wall}}}{r_{\text{beam}}} + \alpha$$

Here, α is between 0 (incompressible beam) and $\frac{1}{2}$ (constant radius beam)

- Acceleration gaps with longitudinally-extended fringing field
 - Idealized waveforms
 - Circuit models including passive elements in “comp boxes”
 - Measured waveforms
- Centroid tracking for studying misalignment effects, steering
- Optimization loops for waveforms & timings, dipole strengths (steering)
- Interactive (Python language with Fortran for intensive parts)

The field model in ASP yields the correct long-wavelength limit

- For hard-edged beam of radius r_b in pipe of radius r_w , 1-D (radial) Poisson eqn gives:

$$\phi(r) = \frac{\lambda}{2\pi\epsilon_0} \begin{cases} \left[\frac{1}{2} \left(1 - \frac{r^2}{r_b^2} \right) + \ln \frac{r_w}{r_b} \right], & r < r_b \\ \ln \left(\frac{r_w}{r} \right), & r_b \leq r < r_w \end{cases}$$

- The axial electric field within the beam is:

$$E_z(r, z) = -\frac{1}{2\pi\epsilon_0} \left\{ \left[\frac{1}{2} \left(1 - \frac{r^2}{r_b^2} \right) + \ln \frac{r_w}{r_b} \right] \frac{\partial \lambda(z)}{\partial z} - \left[1 - \frac{r^2}{r_b^2} \right] \frac{\lambda(z)}{r_b} \frac{\partial r_b}{\partial z} \right\}$$

- For a space-charge-dominated beam in a uniform transport line, $\lambda/r_b^2 \approx \text{const.}$; find:

$$E_z(r, z) = -\frac{g_{\text{scd}}}{4\pi\epsilon_0} \frac{\partial \lambda(z)}{\partial z}; \quad g_{\text{scd}} = 2 \ln \frac{r_w}{r_b}$$

- For an emittance-dominated beam $r_b \approx \text{const.}$; average over beam cross-section, find:

$$\langle E_z \rangle(z) = -\frac{g_{\text{ed}}}{4\pi\epsilon_0} \frac{\partial \lambda(z)}{\partial z}; \quad g_{\text{ed}} = 2 \ln \frac{r_w}{r_b} + \frac{1}{2}$$

- The ASP field equation limits to such a “g-factor” model when the k_{\perp}^2 term dominates
- In NDCX-II we have a space-charge-dominated beam, but we adjust the solenoid strengths to keep r_b more nearly constant; $g_0 = 2 \ln(r_w/r_b) + \alpha$; $0 < \alpha < 1/2$
- In practice we tune α to obtain agreement with Warp results

We employ the drift compression concept twice in NDCX-II

- Initial (non-neutralized) drift compression shortens the pulse for:
 - better use of induction-core Volt-seconds
 - early use of high-voltage Blumlein power supplies (~70 ns limit)



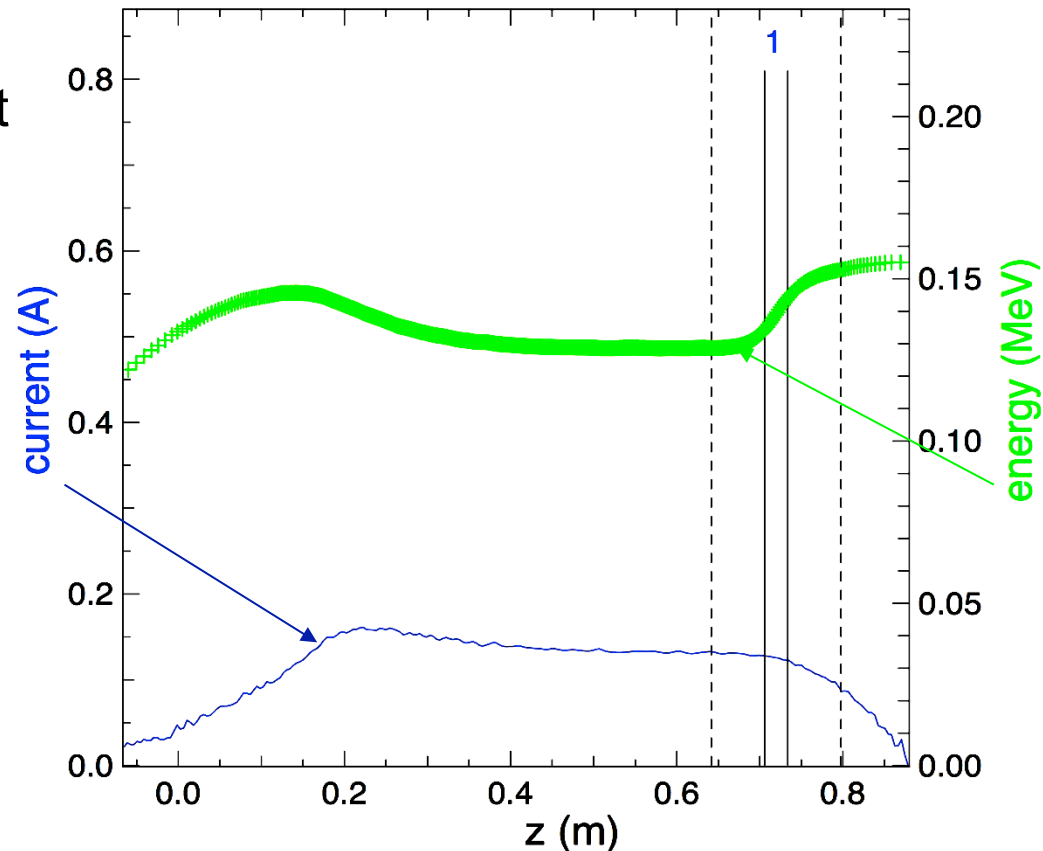
- Final “neutralized drift compression” onto the target
 - Electrons in plasma move to cancel the beam’s electric field
 - Require $n_{\text{plasma}} > n_{\text{beam}}$ for this to work well

NDCX-II design physics: A. Friedman, *et al.*, *Phys. Plasmas* **17**, 056704 (2010).

1-D simulation code ASP (“Acceleration Schedule Program”)

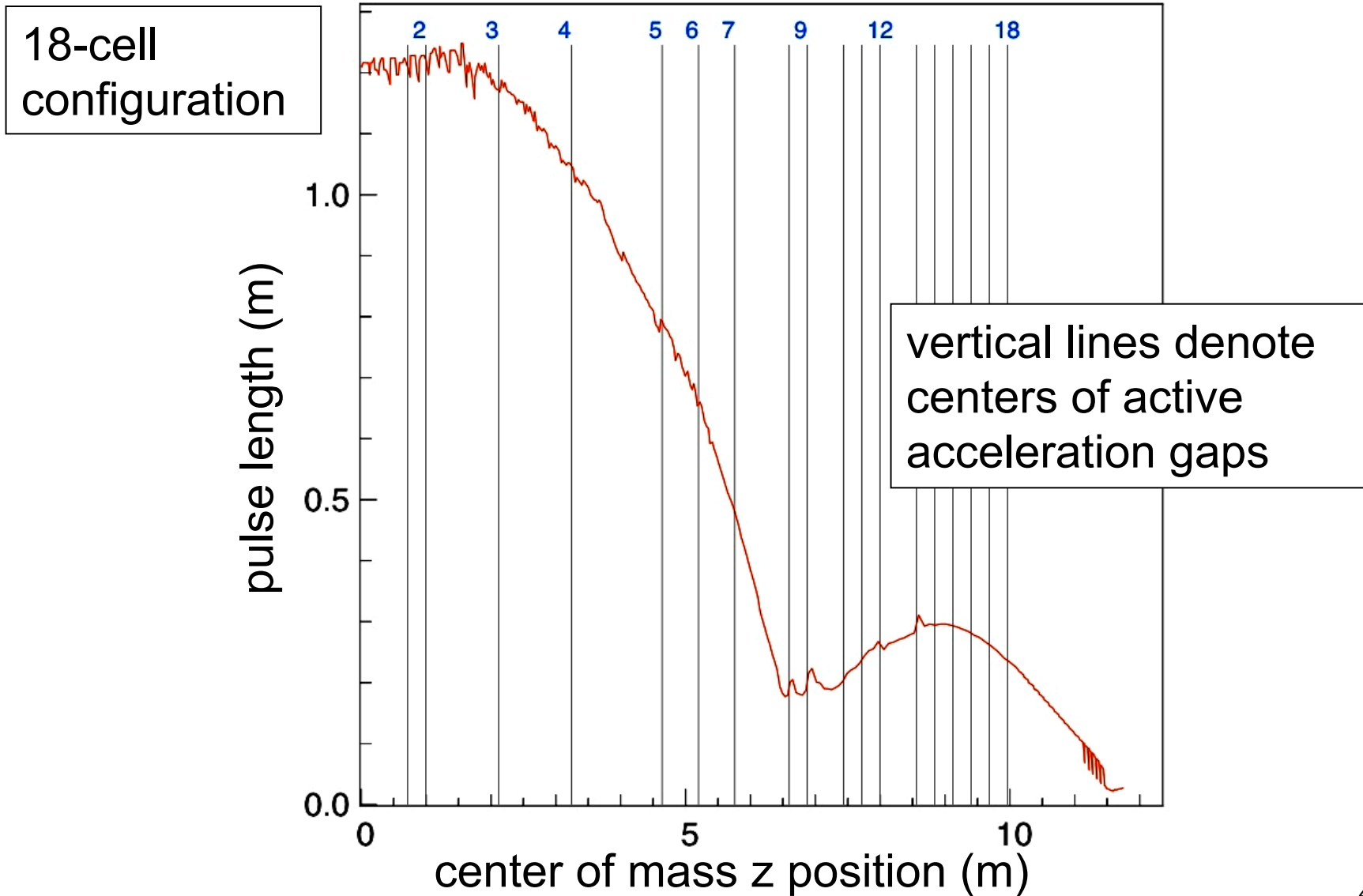
- Follows (z, v_z) phase space using a few hundred particles (“slices”)

“Snapshots” of current and kinetic energy profiles vs. z , 120 ns into a simulated shot:



- Centroid tracking for studying imperfect alignment
- Optimization loops for waveforms & timings, dipole strengths (steering)
- Interactive (Python language with Fortran for intensive parts)

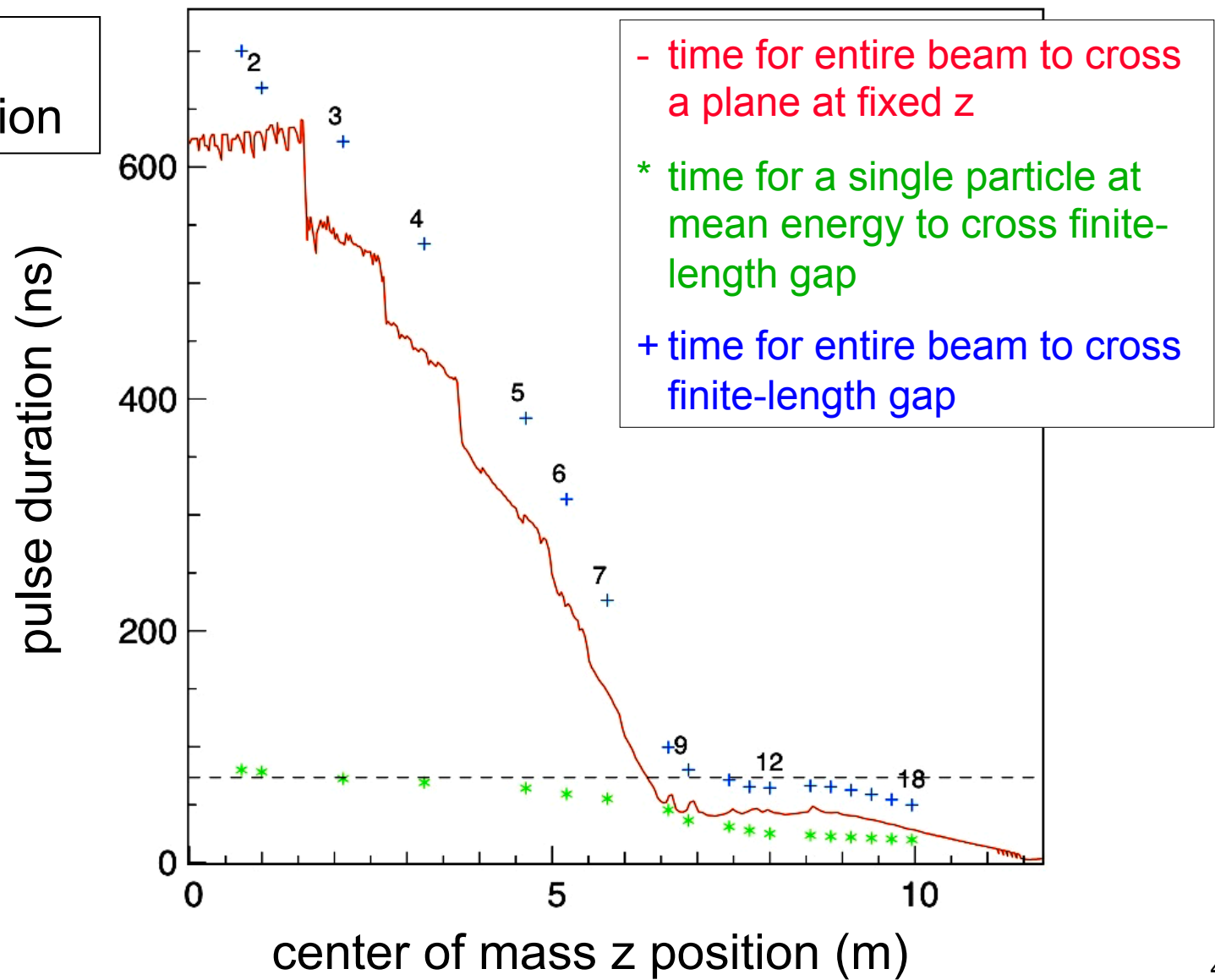
Pulse length vs. z, as developed using 1-D ASP simulation



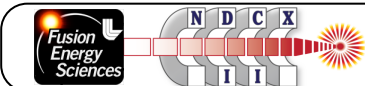
40h.0010-18

Pulse duration vs. z: the entire beam transit time is key

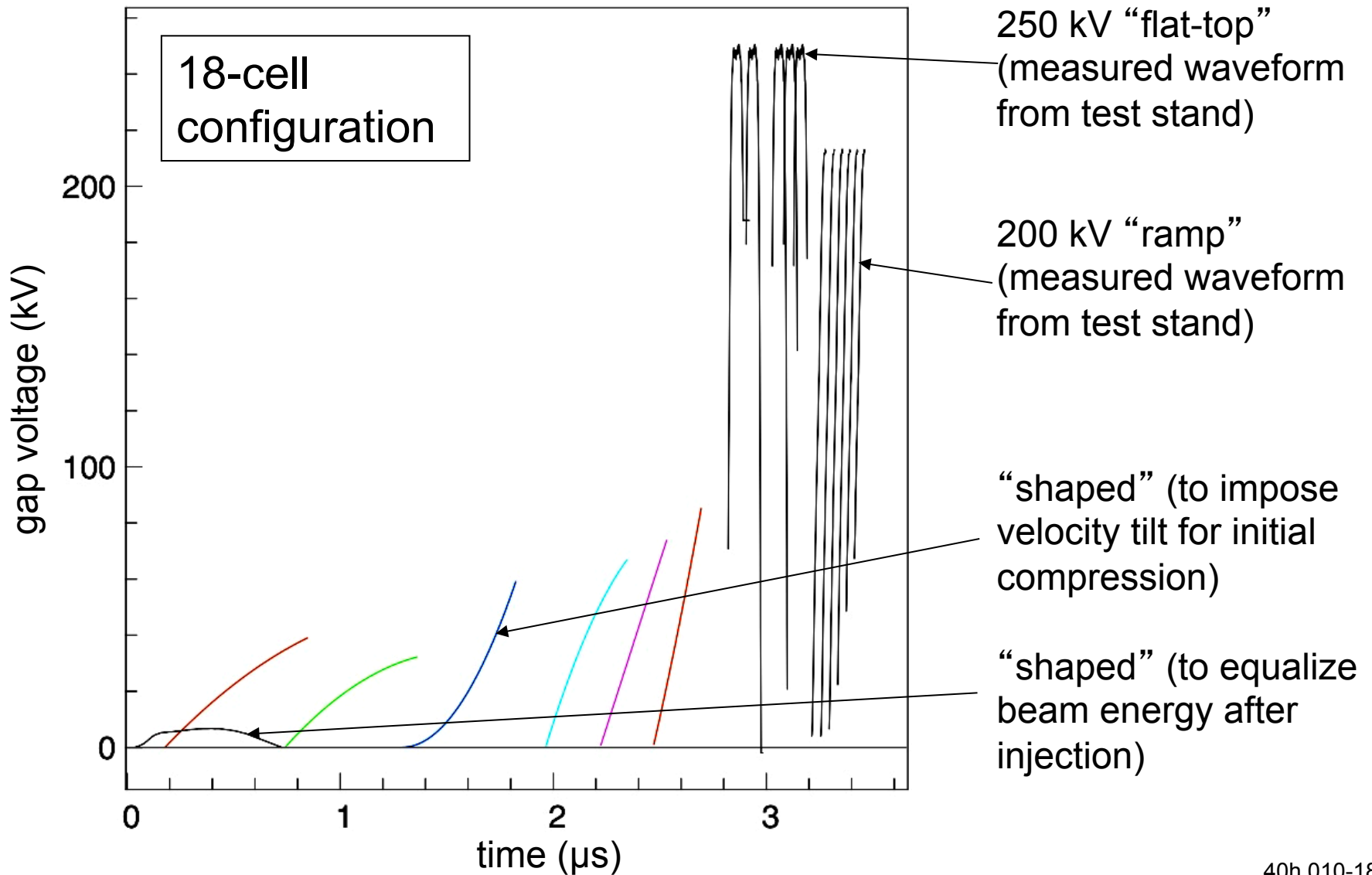
18-cell configuration



40h.010-18



Acceleration waveforms, developed with 1-D ASP PIC code



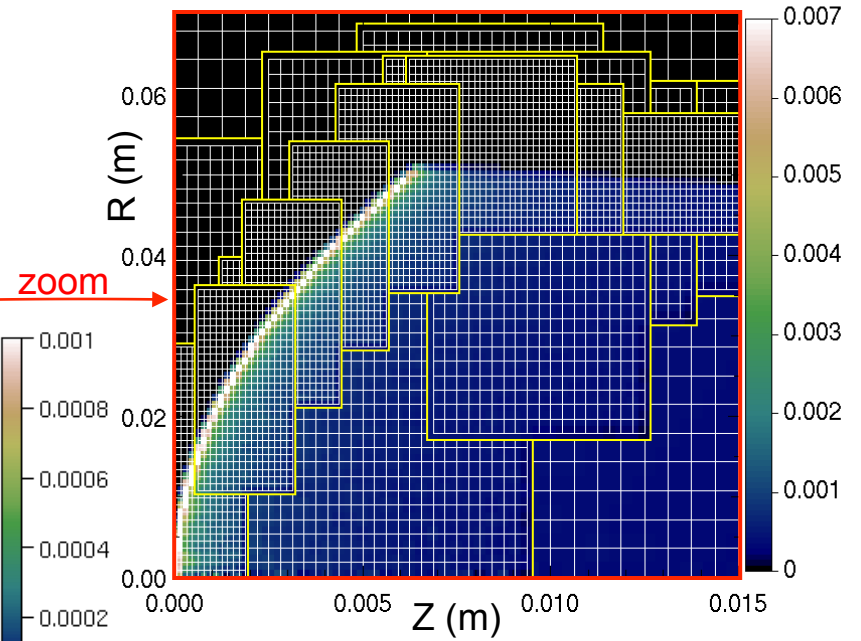
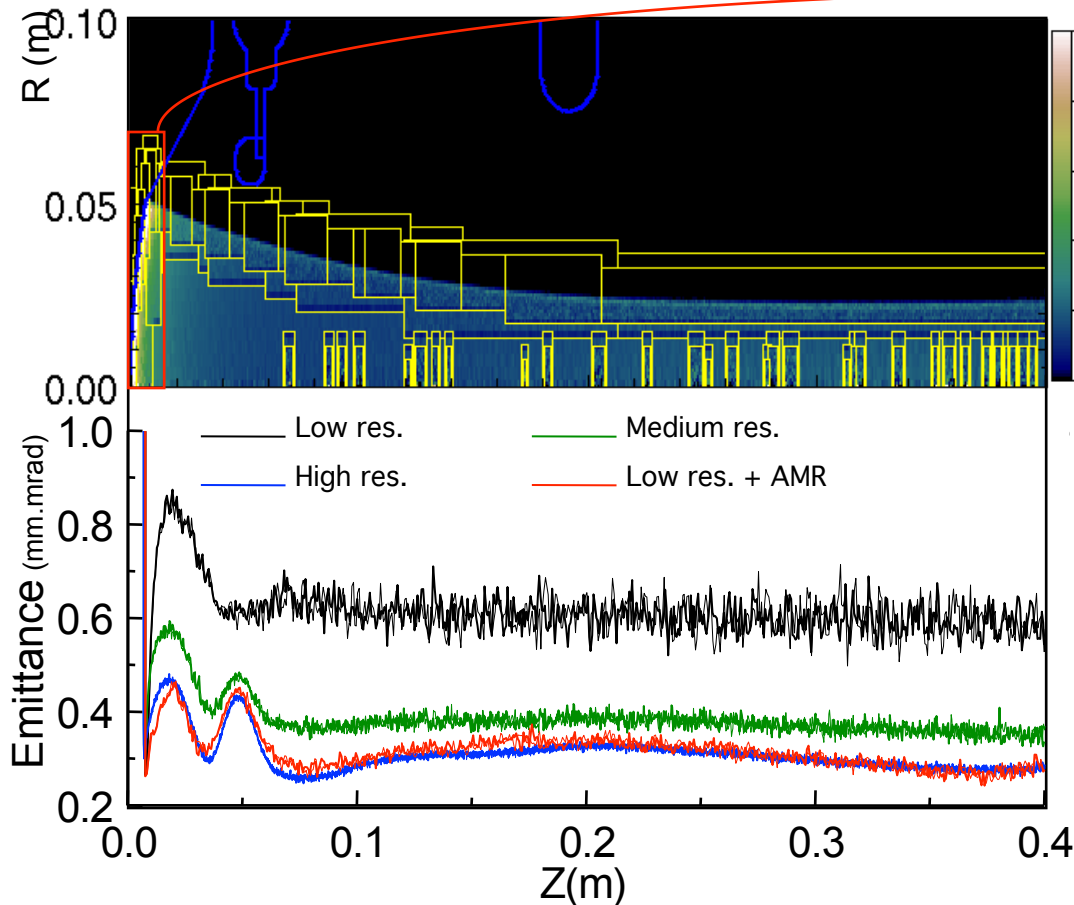
40h.010-18

Warp

- 3-D and axisymmetric (r,z) models
- Electrostatic space charge and acceleration gap fields
- Time-dependent space-charge-limited emission
- Cut cells boundaries, AMR, large-timestep drift-Lorentz mover, ...
- Interactive (Python language)
- Extensively benchmarked against experiments & analytic cases

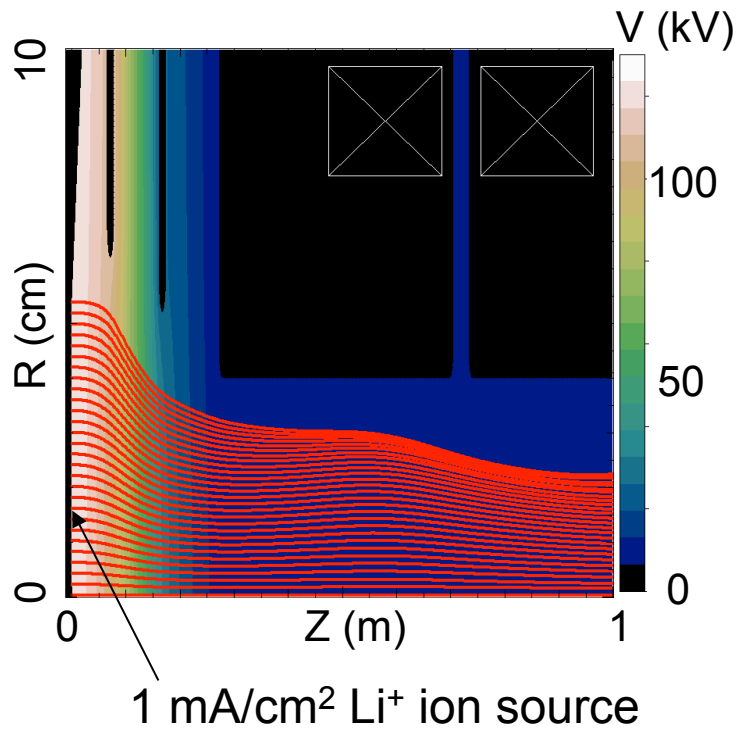
Electrostatic AMR simulation of ion source : speedup x10

Run	Grid size	Nb particles
Low res.	56x640	~1M
Medium res.	112x1280	~4M
High res.	224x2560	~16M
Low res. + AMR	56x640	~1M



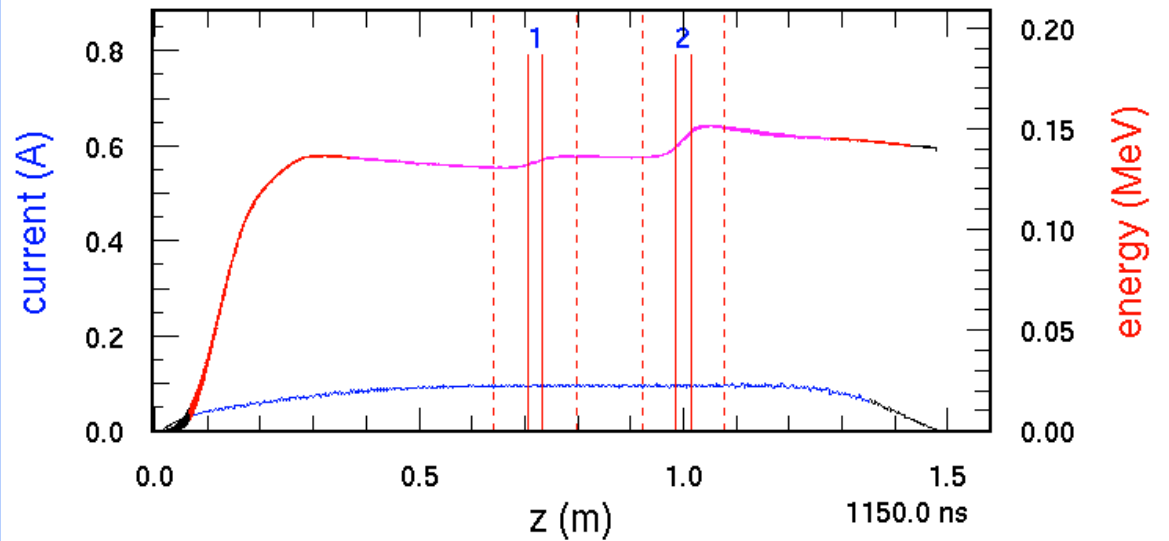
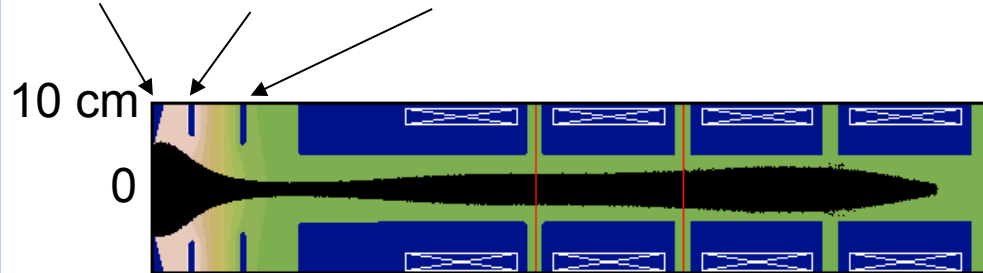
Injector design was developed using Warp in (r,z) geometry

First, used steady-flow “gun” mode to design for a nearly laminar flow:



Second, carried out fully time dependent simulation:

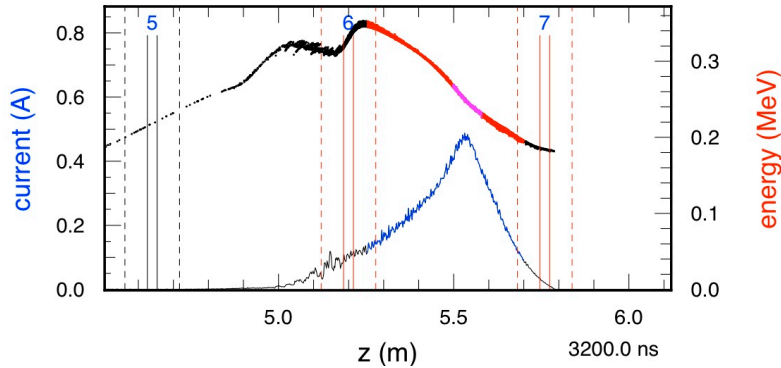
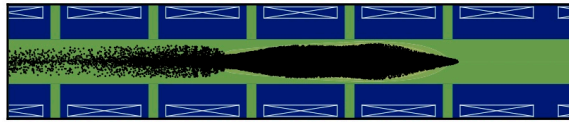
emitter 130 kV extractor 117 kV accel 20 kV (during main pulse)



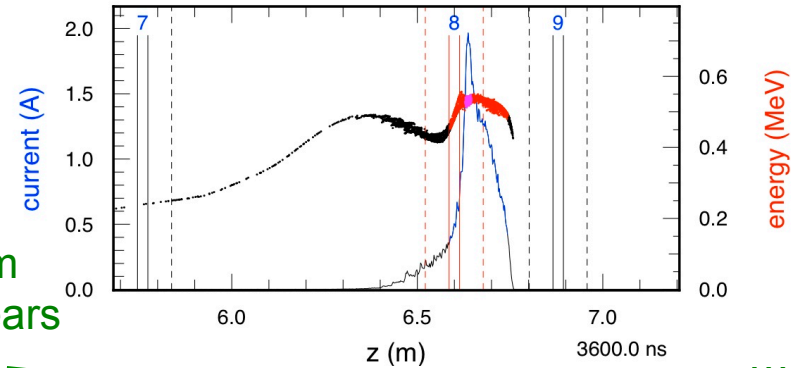
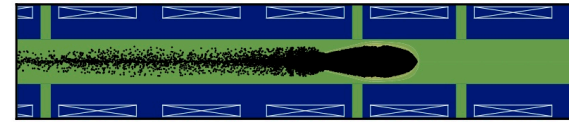
40g-12

Snapshots from a Warp (r,z) simulation (18-cell version)

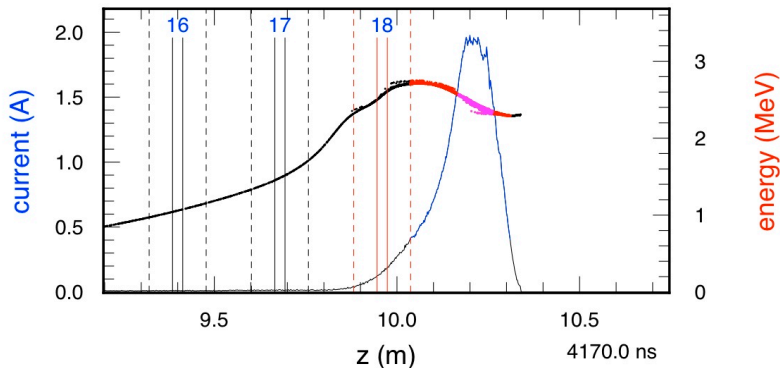
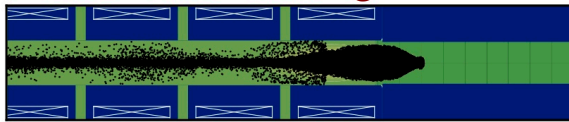
compressing



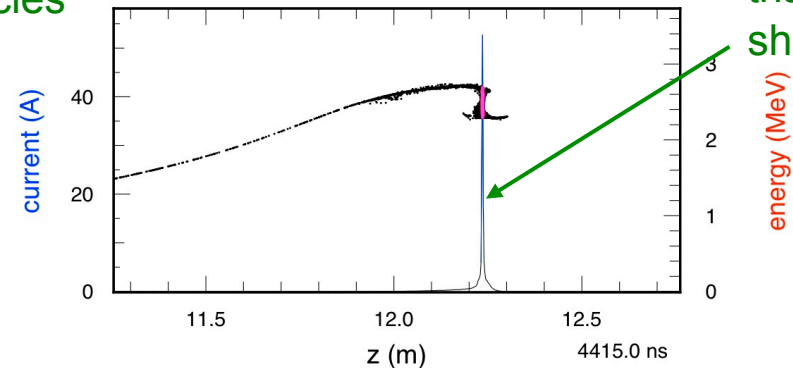
approaching maximum compression



exiting



at focus



Beam appears long because we plot many particles

...

... but current profile shows that it is short

NDCX-II capabilities for supporting experiments will grow

- Currently connecting the Blumleins; drift line, final focus, and target chamber will follow
- We will continue to optimize:
 - brightness and uniformity of the injected beam
 - longitudinal beam manipulations and compression
 - beam steering to correct for residual misalignments
 - beam neutralization and final focusing
- The following are goals for the 12-cell configuration

	Now (no Blumleins, drift, focus)	Near term	Longer term
Charge (in $\sqrt{2}$ x duration)	50 nC	25 nC	50 nC
Ion kinetic energy (MeV)	0.2 MeV	1.2 MeV	1.2 MeV
Focal radius (50% of beam)	N/A	1.5 mm	<1 mm
FWHM Duration	50 ns	1.0 ns	<1 ns
Peak current	0.65 A	5 A	>30 A
Peak fluence	N/A	>1 J/cm ²	>8 J/cm ²

Additional induction cells will significantly enhance performance

- Higher kinetic energy, shorter pulse
- Thus higher target pressures, above many critical points
- More uniform heating (beam slows through Bragg peak while in target)
- For 3 MeV, append 10 lattice periods (we have additional cells from LLNL on hand)

	NDCX-I (bunched beam)	NDCX-II	
		12 active cell (27 periods)	21 active cell (37 periods)
Ion species	K ⁺ (A=39)	Li ⁺ (A=7)	Li ⁺ (A=7)
Charge	15 nC	50 nC	50 nC
Ion kinetic energy	0.3 MeV	1.2 MeV	3.1 MeV
Focal radius (50% of beam)	2 mm	0.6 mm	0.6 mm
Duration (FWHM)	2 ns	0.6 ns	0.3 ns
Peak current	3 A	36 A	86 A
Peak fluence (time integrated)	0.03 J/cm ²	8.6 J/cm ²	22 J/cm ²
Fluence w/in 0.1 mm diameter, w/in duration		5.3 J/cm ²	15 J/cm ²
Max. central pressure in Al target		0.07 Mbar	0.23 Mbar
Max. central pressure in Au target		0.18 Mbar	0.64 Mbar

NDCX-II potential performance for “well tuned” configurations

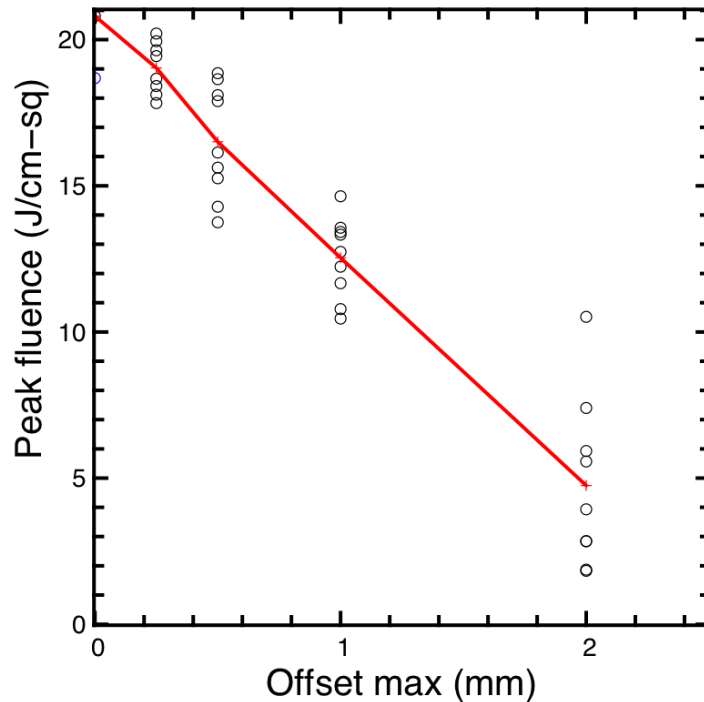
	NDCX-I (bunched beam)	NDCX-II construction project			NDCX-II 21-cell (enhanced)
		12-cell (baseline)	15-cell (“probable”)	18-cell (“possible”)	
Ion species	K ⁺ (A=39)	Li ⁺ (A=7)	Li ⁺ (A=7)	Li ⁺ (A=7)	Li ⁺ (A=7)
Total charge	15 nC	50 nC	50 nC	50 nC	50 nC
Ion kinetic energy	0.3 MeV	1.2 MeV	1.7 MeV	2.4 MeV	3.1 MeV
Focal radius (50% of beam)	2 mm	0.6 mm	0.6 mm	0.6 mm	0.7 mm
Duration (bi-parabolic measure = $\sqrt{2}$ FWHM)	2.8 ns	0.9 ns	0.4 ns	0.3 ns	0.4 ns
Peak current	3 A	36 A	73 A	93 A	86 A
Peak fluence (time integrated)	0.03 J/cm ²	13 J/cm ²	19 J/cm ²	14 J/cm ²	22 J/cm ²
Fluence w/in 0.1 mm diameter, w/in duration		8 J/cm ²	11 J/cm ²	10 J/cm ²	17 J/cm ²
Max. central pressure in Al target		0.07 Mbar	0.18 Mbar	0.17 Mbar	0.23 Mbar
Max. central pressure in Au target		0.18 Mbar	0.48 Mbar	0.48 Mbar	0.64 Mbar

Caveats: these are from (r,z) Warp runs (no misalignments), and assume uniform 1 mA/cm² emission, front-end pulses that match the design, and perfect neutralization; they use only measured Blumlein waveforms

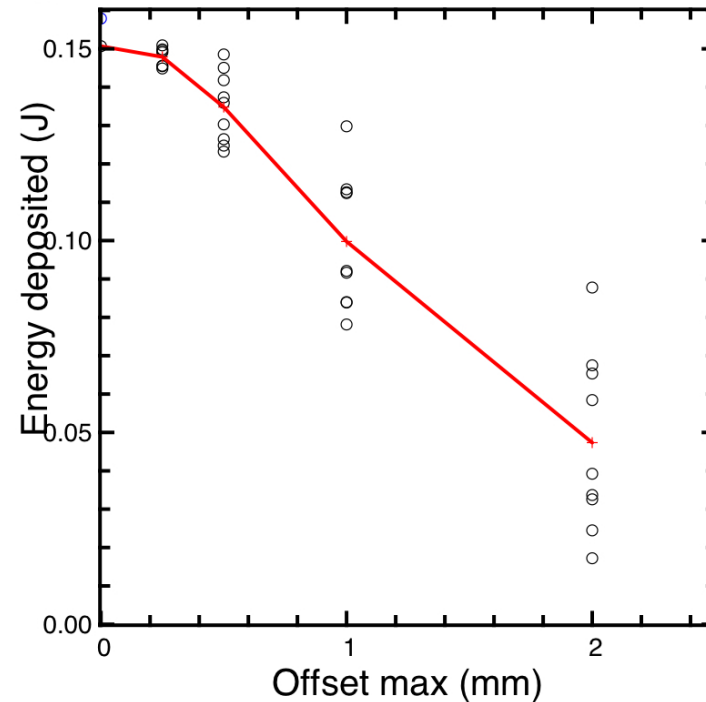
Warp 3D simulations indicate slow degradation of the focus as misalignment of the solenoids increases

- Random offsets in x and y were imparted to the solenoid ends.
- The offsets were chosen from a uniform distribution with a set maximum.

Peak deposition

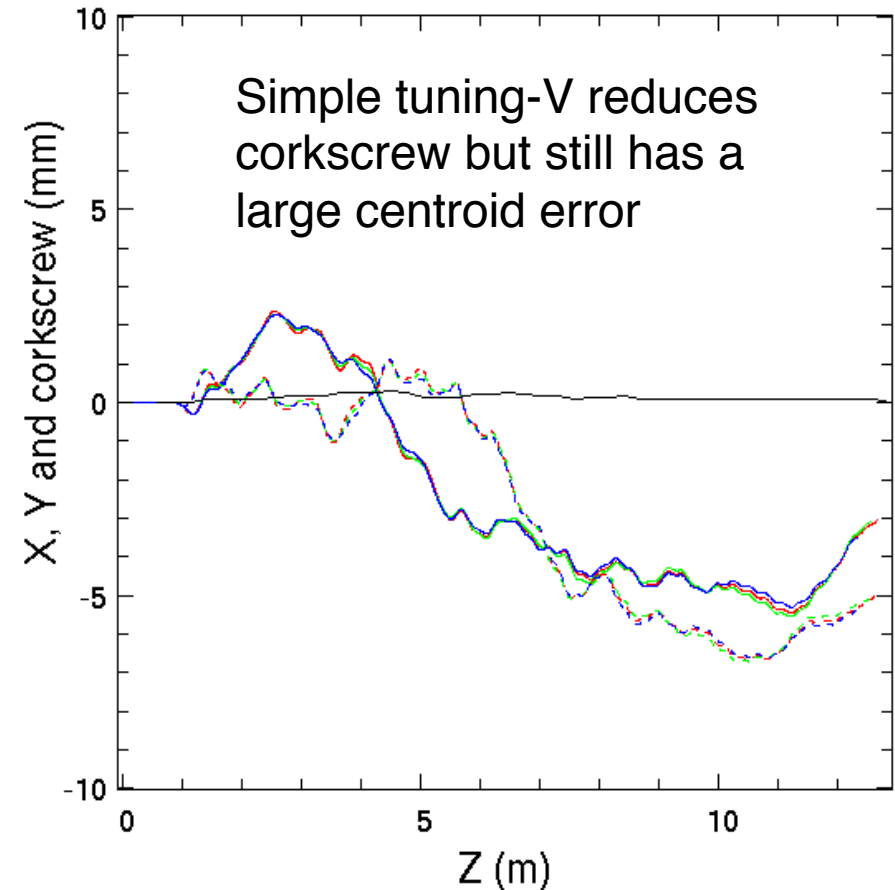
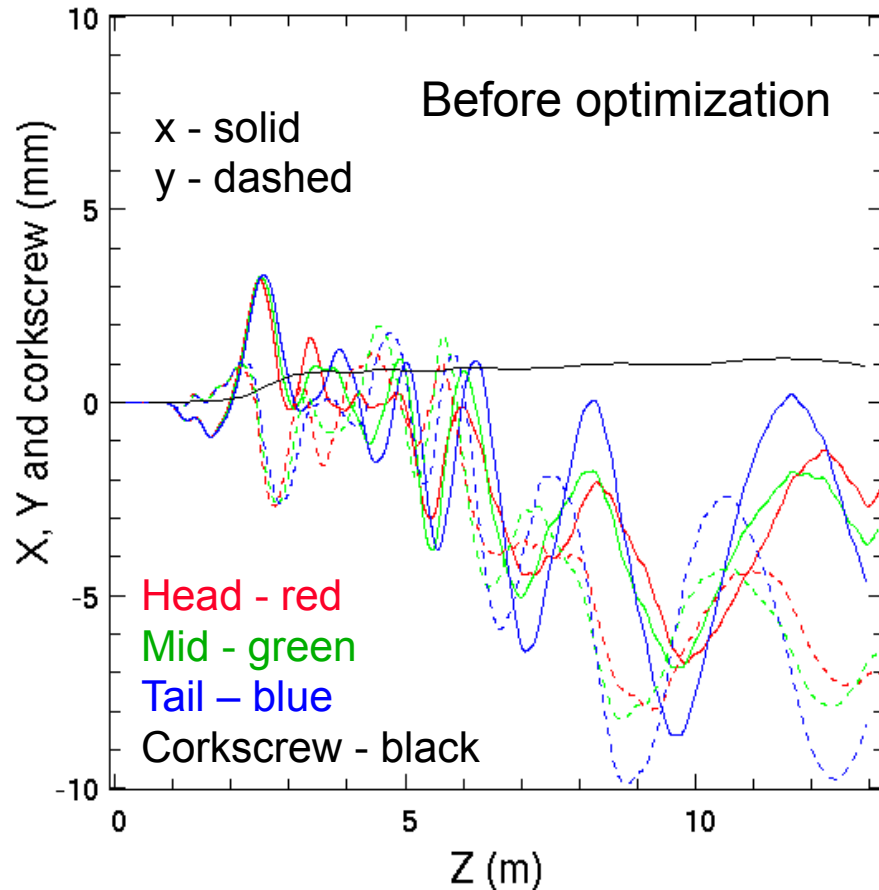


Energy deposited within 1 mm of the location of the peak



“Tuning V” algorithm (modeled in ASP) adjusts “steering” dipole currents so as to minimize a penalty function at the next sensor

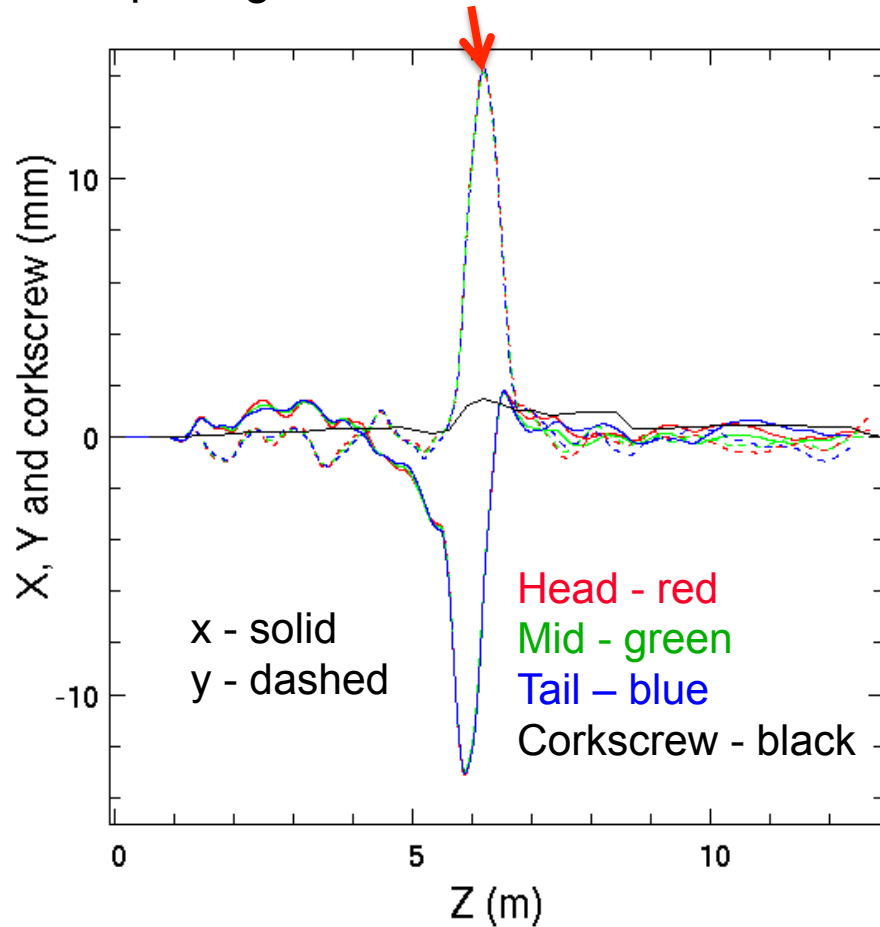
x,y vs z trajectories of head, mid, tail particles and the corkscrew size for a typical ASP run



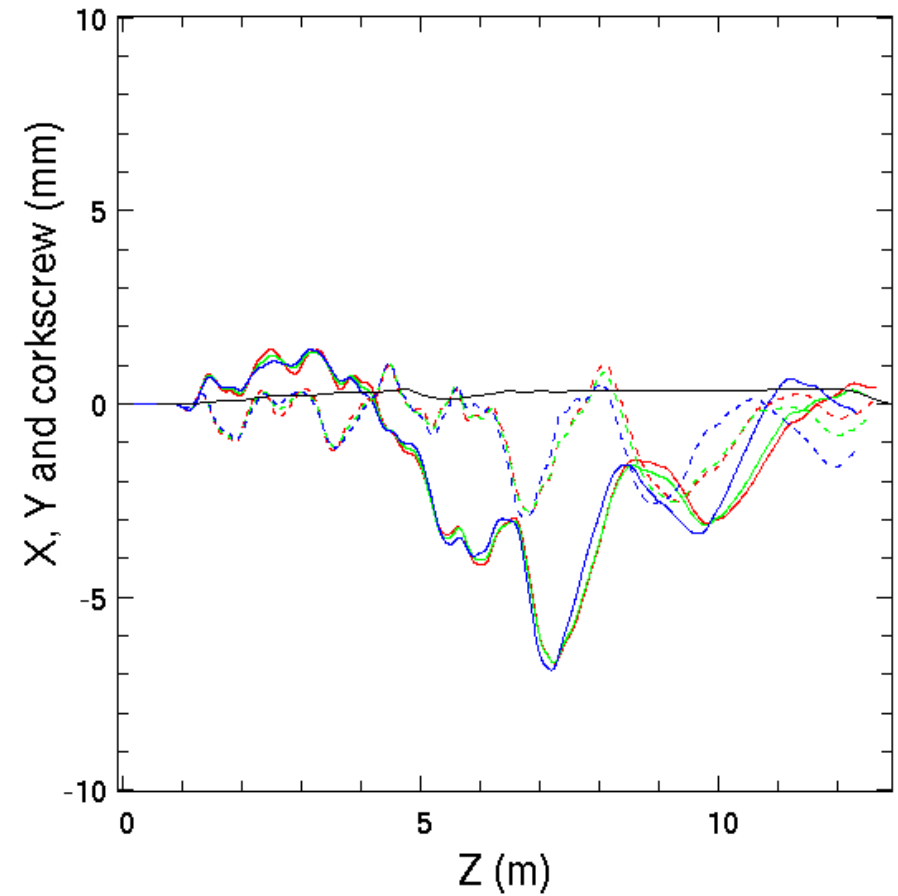
Random offsets of solenoid ends up to 1 mm were assumed; the effect is linear.

Beam offset can be added to penalty, but care is needed

Resonance occurs between sensor spacing and centroid oscillation

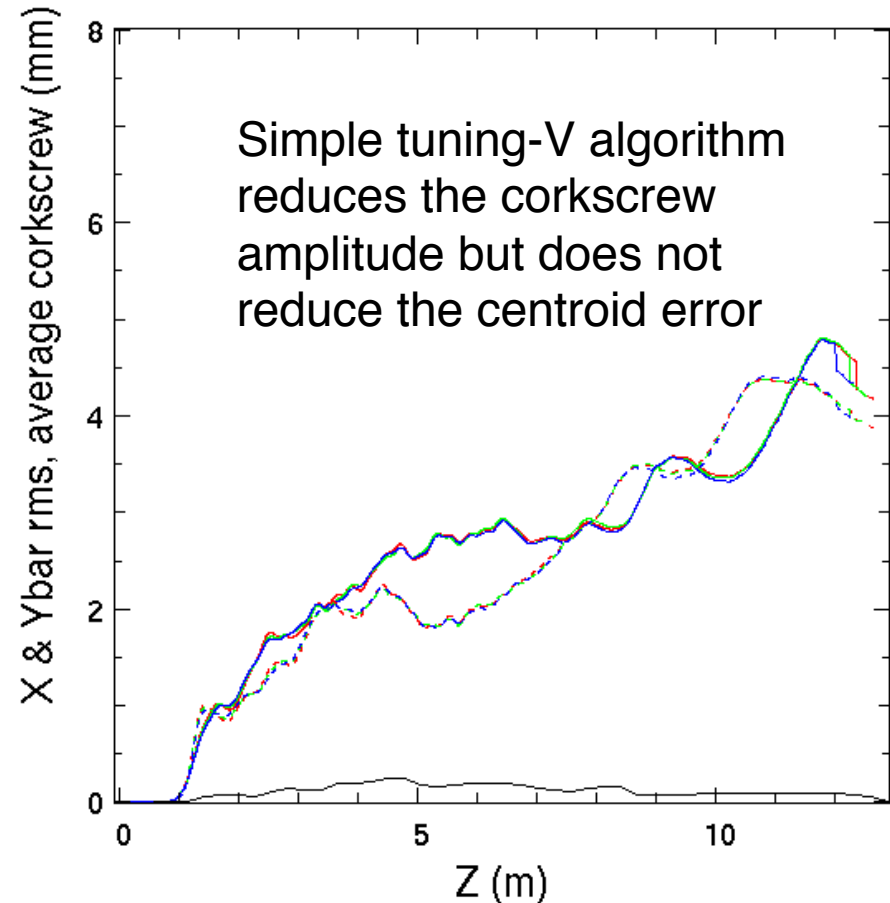
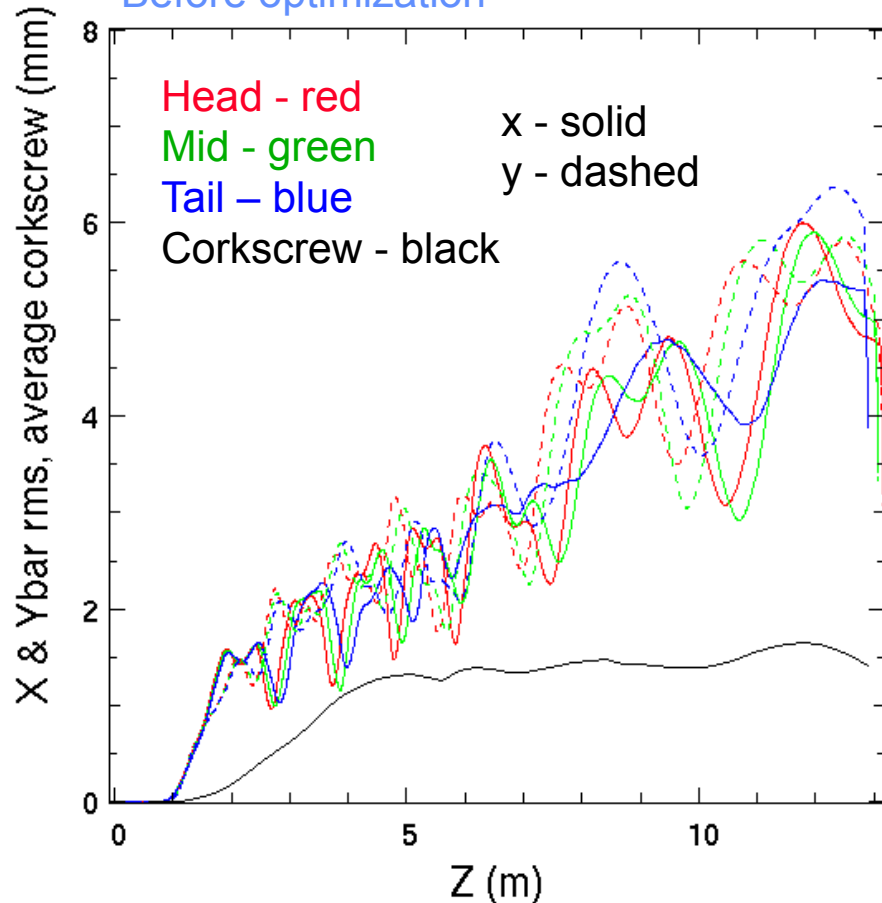


Constraining the dipole strength to < 100 Gauss reduces the peak



An ensemble of runs shows the same trends

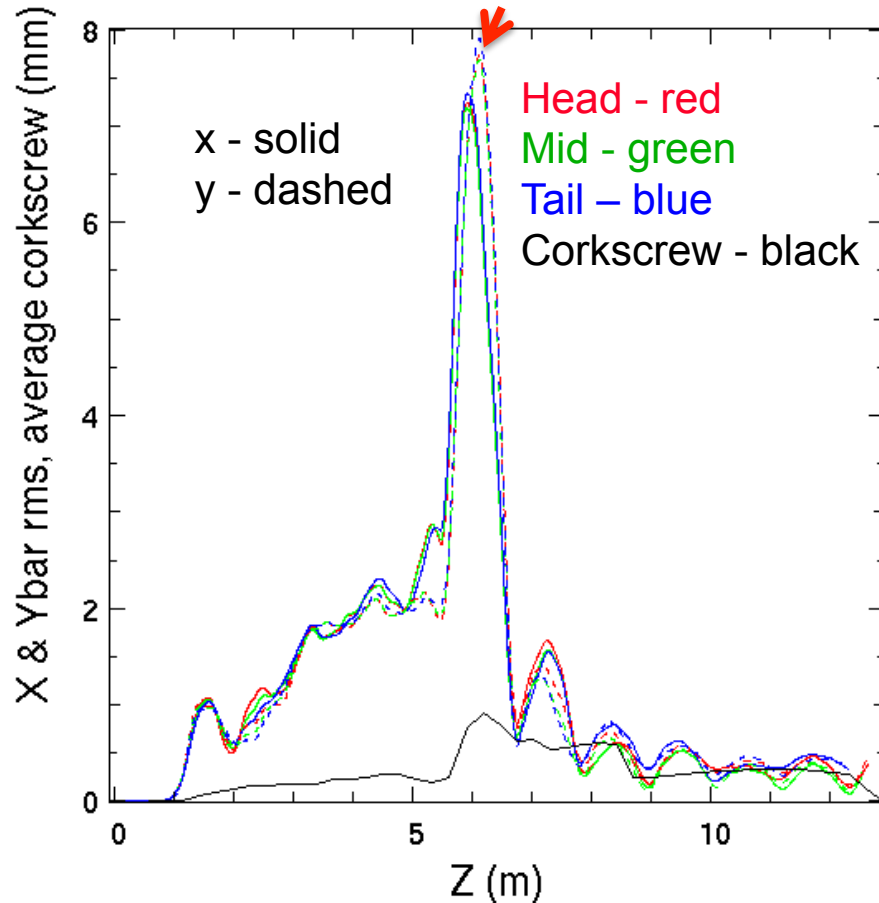
x,y vs z trajectories of head, mid, tail particles and the corkscrew amplitude
Before optimization



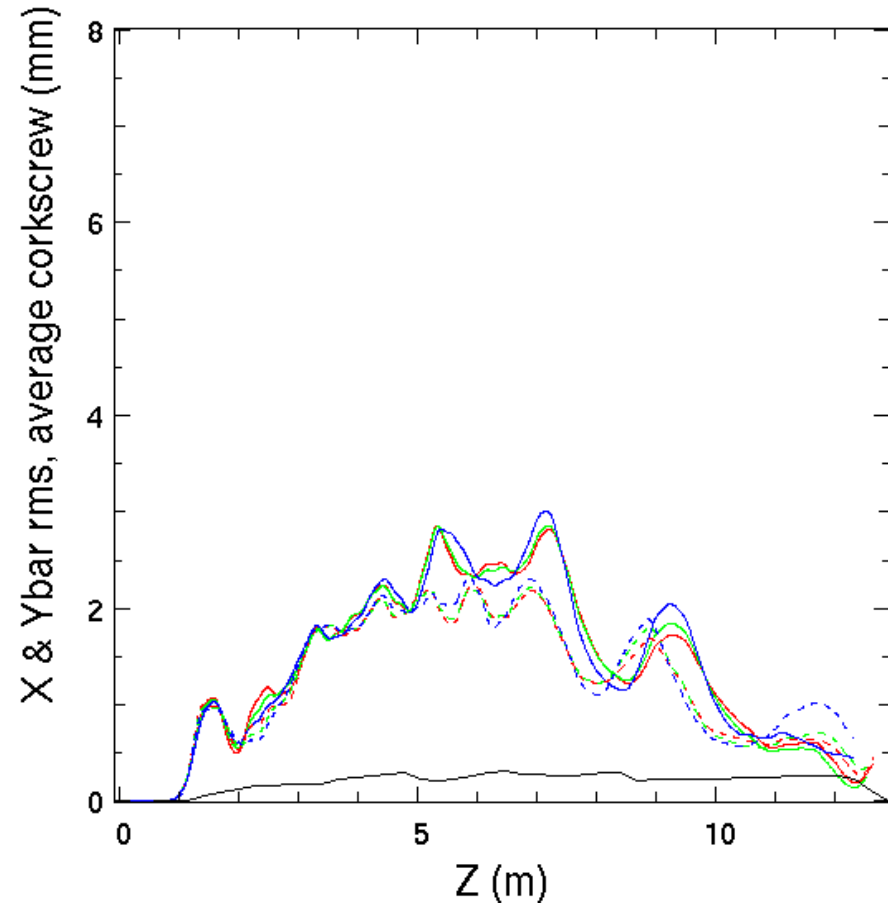
The results are averages over 20 simulations with differing random offsets of solenoid ends up to 1 mm.

The effects of penalizing the beam offset and dipole strength are clearer when an ensemble of runs is examined

Resonance between sensor spacing and cyclotron oscillation spatial period



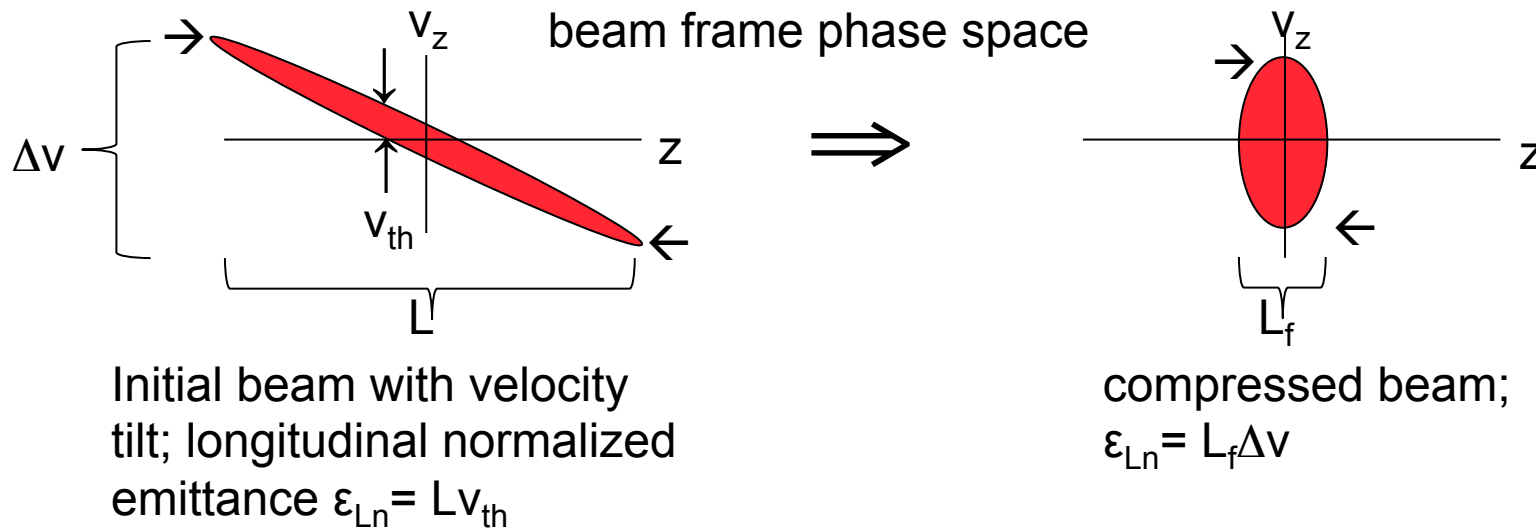
Constraining the dipole strength to < 100 Gauss removes the peak



NDCX-II will be an exciting platform for beam physics studies (many of them relevant to an HIF driver)

- **NDCX-II operation embodies collective beam dynamics:**
 - Driver-like compression of non-neutral and neutralized beams
 - Space charge-driven removal of velocity tilt, to achieve “stagnation”
 - Longitudinal waves are evident
- **Non-ideal effects include:**
 - Emittance growth (phase-space dilution), “halo” formation
 - Beam - plasma interactions and instabilities
 - Aberrations in final focus
- **Add-on hardware could enable studies of:**
 - Collective focusing of ion beams
 - Intense beam transport in quadrupoles
 - Beam dynamics in bends
- **Beam diagnostics will be developed and improved**

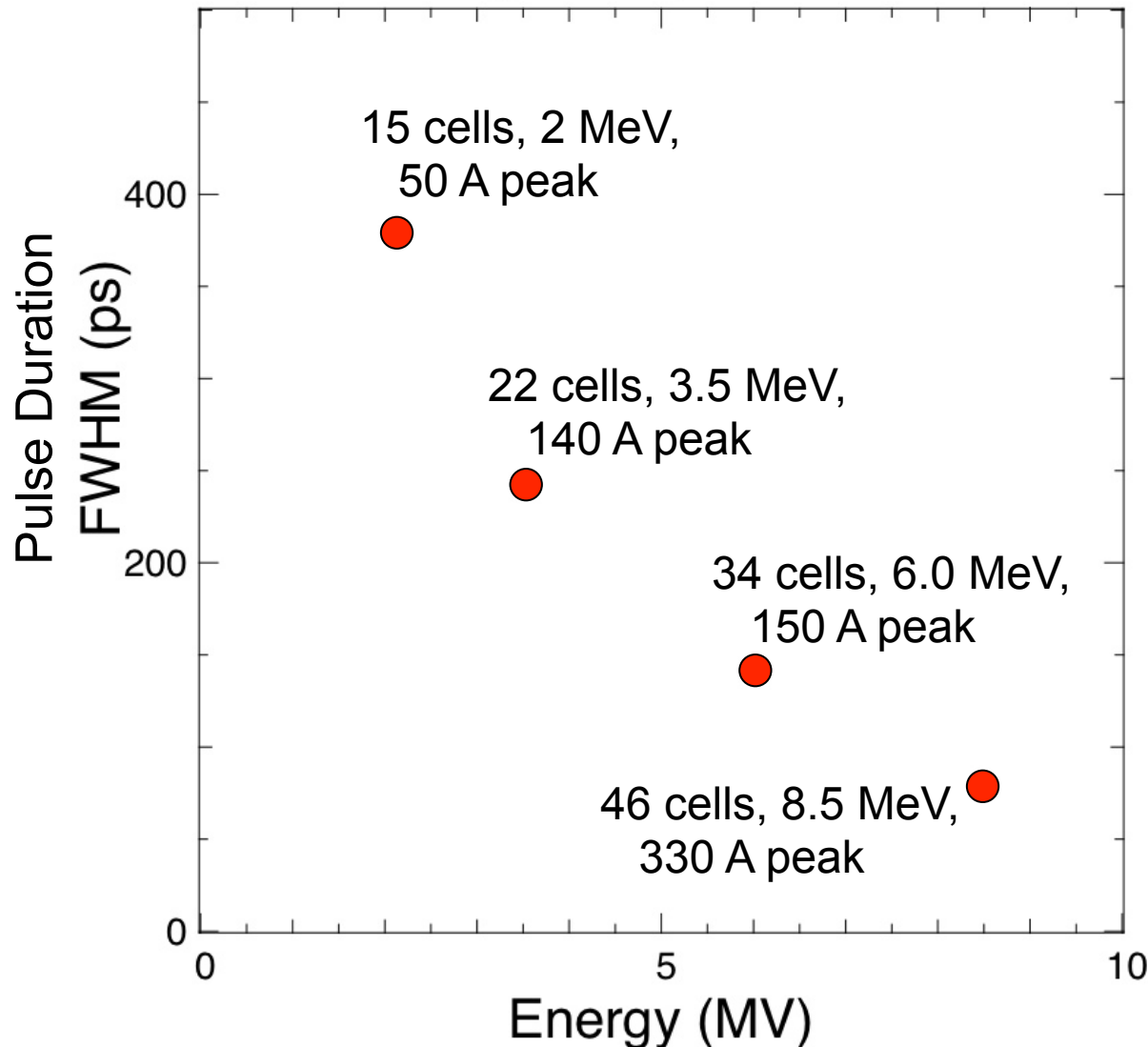
Accelerating to higher kinetic energy permits neutralized drift compression to a shorter final pulse duration



- With ideal accelerating waveforms ϵ_{Ln} (shaded area) is conserved
- With our waveforms it is nearly conserved
- ϵ_{Ln} is thus mostly set by distortions imparted to the beam early-on
- The final duration τ_f decreases with the velocity v and velocity variation Δv :

$$\tau_f = L_f / v = (\epsilon_{Ln} / \Delta v) (1/v)$$
- For larger v , we can tolerate a larger Δv . The scaling seen in Warp simulations of NDCX-II with increasing number of induction cells is close to $\tau_f \sim v^{-2}$
- Random errors in acceleration waveforms & timing do not alter these conclusions

Assuming ideal neutralization, pulse duration in NDCX-II varies roughly inversely with kinetic energy — with 46 induction cells, beam phase space appears consistent with ~ 100 ps FWHM



Results of Warp simulations, using highly optimized waveforms and assuming ideal pulse timing, voltage accuracy, neutralization, and source uniformity

- Separate studies have examined effects of:
 - timing jitter and voltage ripple in accelerating waveforms
 - injector voltage ripple
 - misalignments
 - source emission (2 mA/cm^2 assumed here)
 - source temperature
- Modest degradation due to these effects is observed

For beam dynamics, a key parameter is the “perveance”

- The dimensionless perveance K is:
where λ is the line charge density
$$K = \frac{2q\lambda}{4\pi\epsilon_0 m v^2} = \frac{2q\lambda}{10^7 m \beta^2} .$$
- K is a measure of how rapidly an unconfined beam would blow up to \sim twice its initial radius: $L_{blowup} / \text{radius} = 1 / \sqrt{K}$
- Formula:
$$K = \frac{1}{4\pi\epsilon_0} \left(\frac{m}{2q} \right)^{1/2} \frac{I}{(V)^{3/2}} = 649,360 \left(\frac{A}{Z} \right)^{1/2} \frac{I}{(V)^{3/2}}$$
- Most accelerators have “emittance dominated” beams: the primary transverse force balance is between thermal pressure and applied confining force
They have perveances of 10^{-5} , often much less
- For our “space charge dominated” beams, the primary force balance is between the beam’s self-field and the applied focusing
- NDCX-II has (transient) peak perveance of 0.01, much greater than the $10^{-5} - 10^{-3}$ for typical driver designs

Self-Focusing Force Estimates for NDCX-I and NDCX-II

Let's compare the self-focusing and magnetic focusing provided by the final focus solenoid (FFS)

Self-focusing

$$F_{self} = m_e V_b^2 \frac{1}{n_p} \frac{dn_b}{dr}$$

$$(\alpha = \omega_{ce} / 2\beta\omega_{pe} \gg 1)$$

FFS focusing

$$F_{sol} = \frac{m_i \omega_{ci}^2 r_b}{4}$$

Focusing strength ratio:

$$\delta = \frac{F_{self} L_d}{F_{sol} L_{FFS}}$$

L_d - length of the drift region

L_{FFS} - solenoid length

NDCX-II (drift section)

$$n_p \sim 10^{11} \text{ cm}^{-3}, m_i = 7 \text{ a.u.}, \beta_b = 0.032$$

$\alpha = 1$ corresponds to $B = 65 \text{ Gs}$

$$L_{FFS} = 10 \text{ cm}, L_d = 200 \text{ cm}, r_b = 1 \text{ cm}$$

$$B_{FFS} = 8 \text{ T}$$

Assume $n_b \sim n_p$

$$\delta = 0.47$$

NDCX-I (drift section)

$$n_p \sim 10^{11} \text{ cm}^{-3}, m_i = 39 \text{ a.u.}, \beta_b = 0.004$$

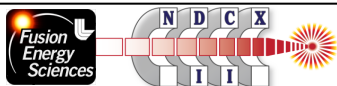
$\alpha = 1$ corresponds to $B = 8 \text{ Gs}$

$$L_{FFS} = 10 \text{ cm}, L_d = 200 \text{ cm}, r_b = 1 \text{ cm}$$

$$B_{FFS} = 8 \text{ T}$$

Assume $n_b \sim n_p$

$$\delta = 0.04$$



Things we need to measure, and the diagnostics we' ll use

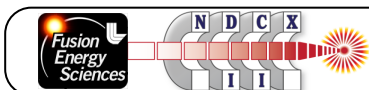
Non-intercepting (in multiple locations):

- Accelerating voltages: voltage dividers on cells
- Beam transverse position: four-quadrant electrostatic capacitive probes
- Beam line charge density: capacitive probes
- Beam mean kinetic energy: time-of-flight to capacitive probes

Intercepting (in two special “inter-cell” sections):

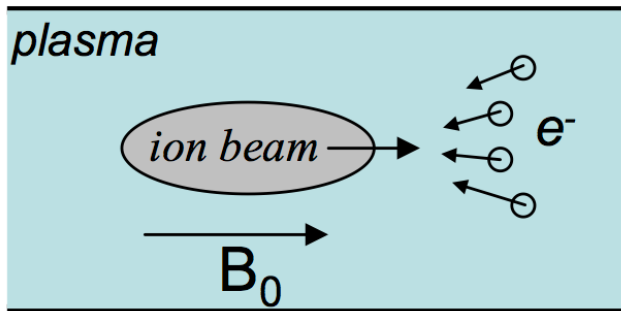
- Beam current: Faraday cup
- Beam emittance: two-slit or slit-scintillator scanner
- Beam profile: scintillator-based optical imaging
- Beam kinetic energy profile: time-of-flight to Faraday cup
- Beam energy distribution: electrostatic energy analyzer

(Underlined items will be available at commissioning)



Beam self-focusing force is greatly enhanced, relative to magnetic self-pinching, by a weak solenoid B field (~100 G)

The enhanced focusing is provided by a strong radial electric field that arises due to a local polarization of the magnetized plasma background by the moving ion beam.



Provided the beam current is neutralized, i.e., $Z_b n_b v_b = n_e v_{ez}$:

$$F_r = Z_b^2 m_e v_b^2 \frac{1}{n_e} \frac{dn_b}{dr}$$

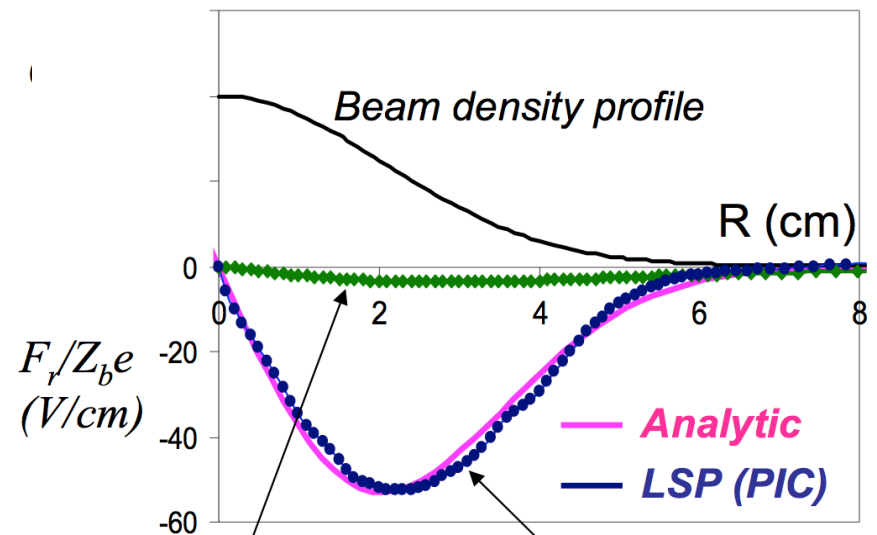
Relative focusing strengths:

NDCX-I: $F_r L_{\text{drift}} / F_{\text{sol}} L_{\text{sol}} \sim 0.04$

NDCX-II: $F_r L_{\text{drift}} / F_{\text{sol}} L_{\text{sol}} \sim 0.5$

M. Dorf, et al., PRL 103, 075003 (2009)

Radial focusing force



$B_{\text{ext}}=0$ $B_{\text{ext}}=300 \text{ G}$
 Magnetic self-pinching Collective self-focusing

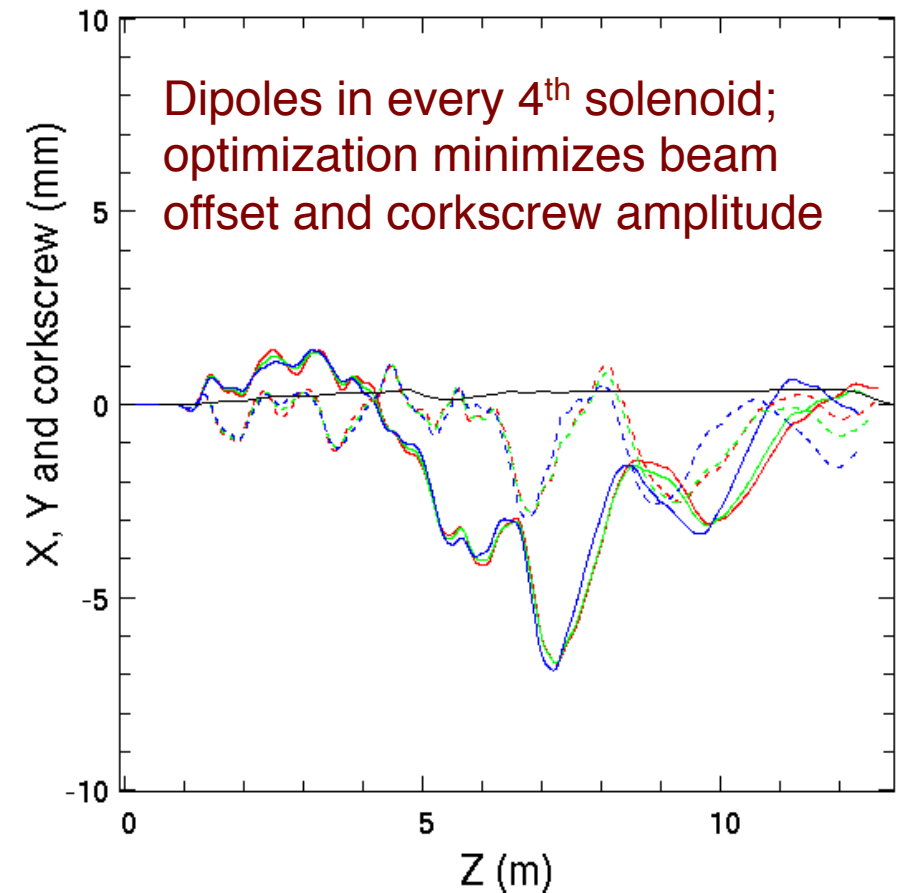
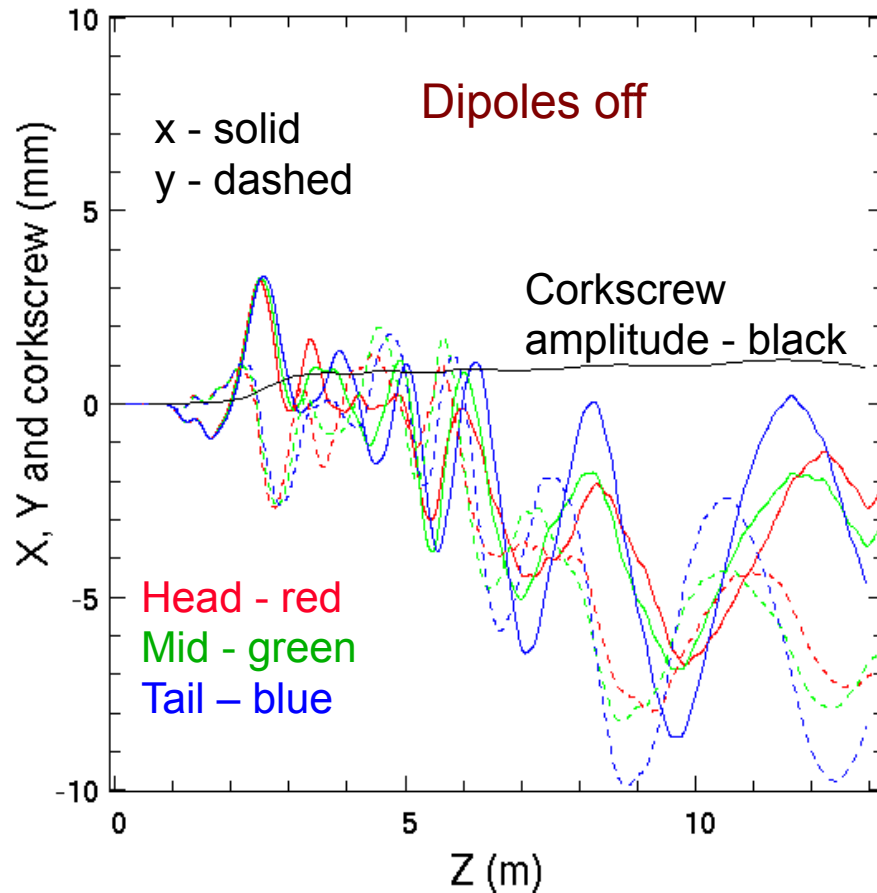
requires:

$$r_{ge} \ll r_b \ll c/\omega_{pe} \quad r_{ge} \equiv \frac{v_b}{\omega_{ce}} \left(1 + \frac{\omega_{ce}^2}{\omega_{pe}^2} \right)^{1/2}$$

$\rightarrow \omega_{ce} \gg 2\beta_b \omega_{pe}$

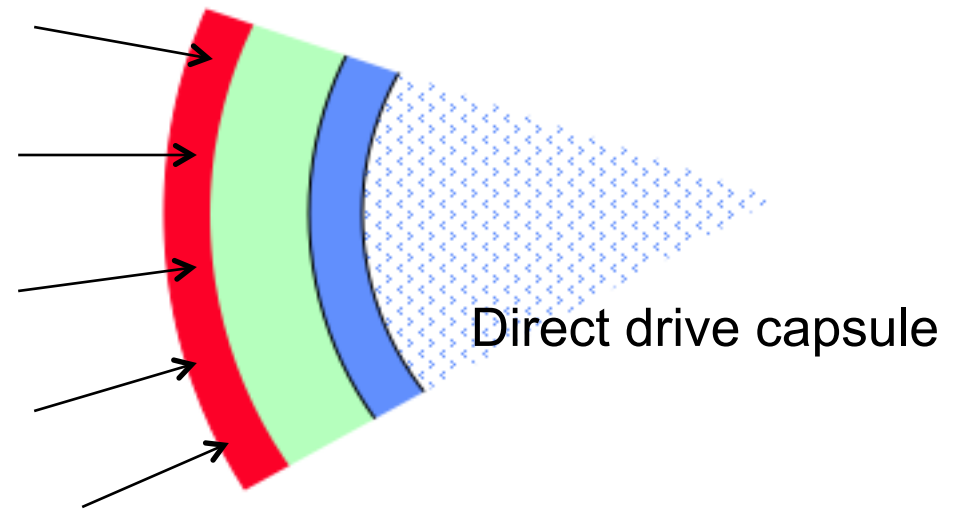
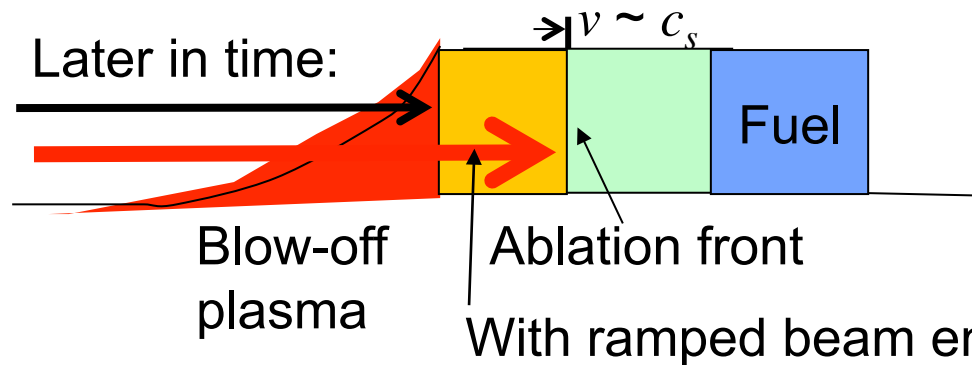
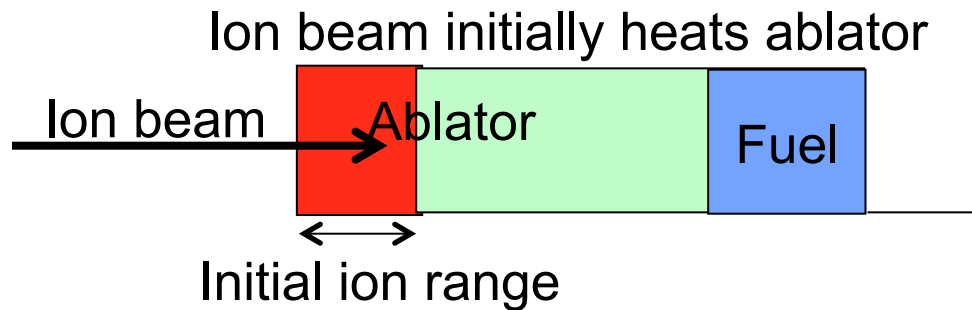
To assess steering, we again used the fast ASP code; a tuning algorithm (as in ETA-II, DARHT)[‡] adjusts dipole strengths

Trajectories of head, mid, tail particles, and corkscrew amplitude, for a 34-cell ASP run. Random offsets of solenoid ends up to 1 mm were assumed; the effect is linear.



[‡] Y-J. Chen, Nucl. Instr. and Meth. A **398**, 139 (1997).

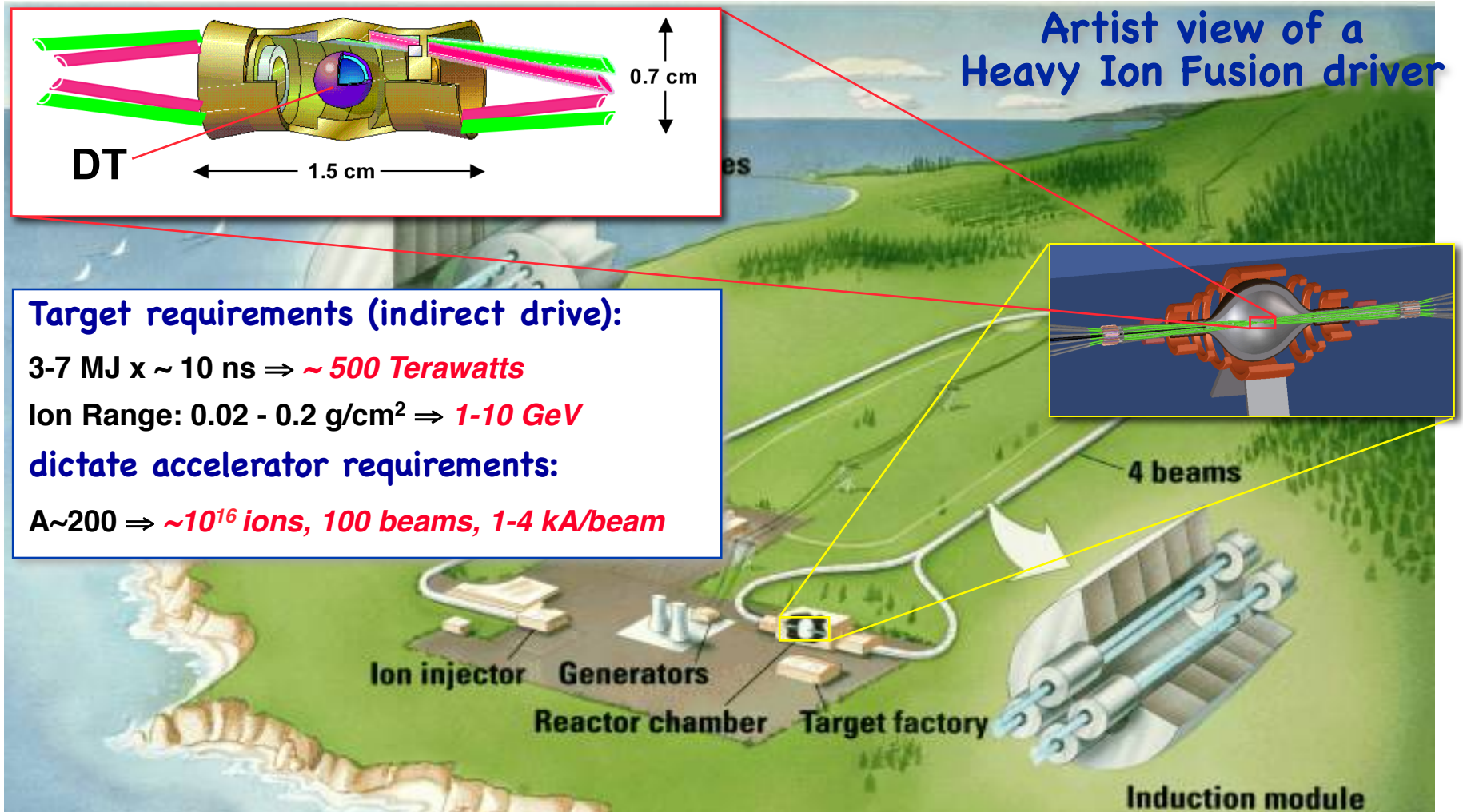
NDCX II will enable study of ion beam coupling physics for high-gain direct drive Inertial Fusion Energy targets



Ablation front would separate from location where energy is deposited
==> Potential low coupling efficiency

Ramping the ion beam energy during the pulse lengthens the stopping range, for efficient coupling of beam energy into motion of the fuel shell

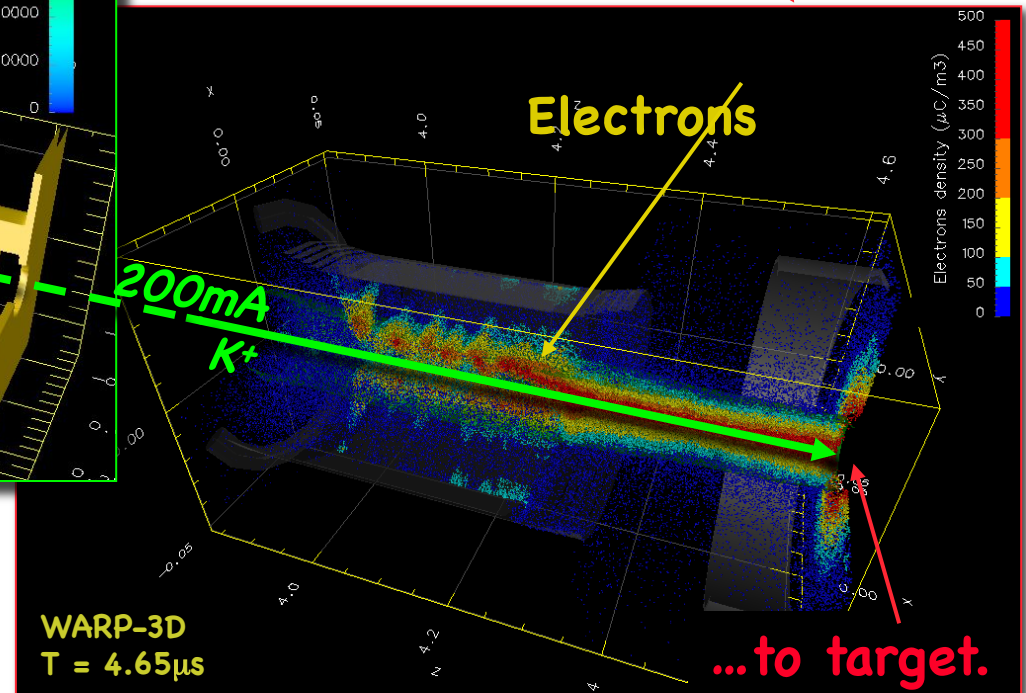
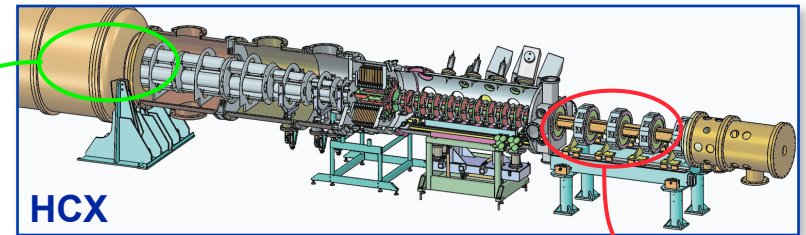
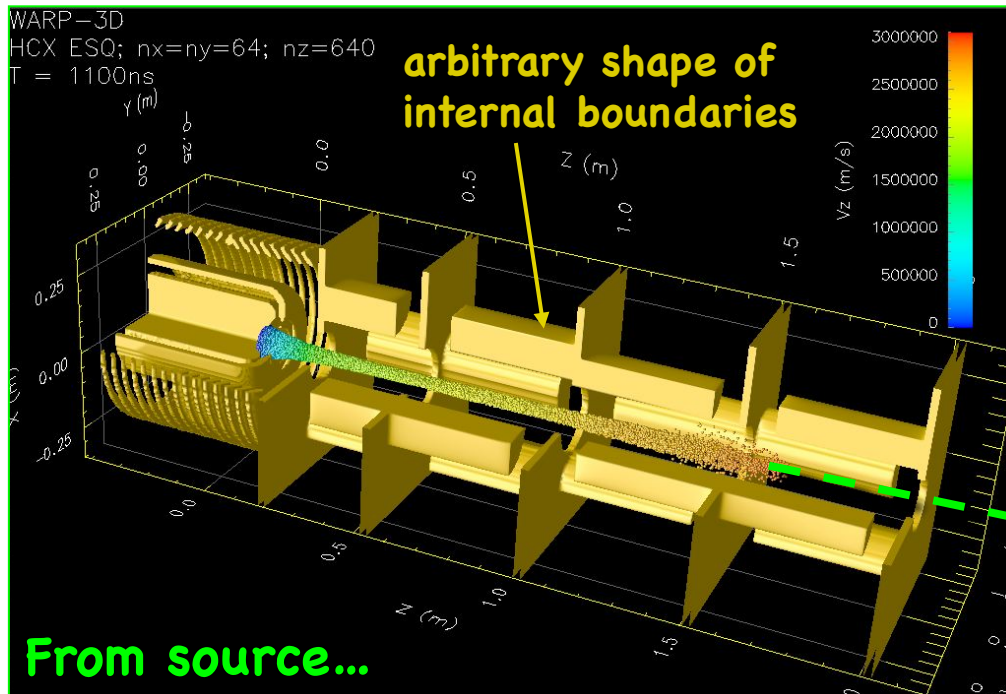
Heavy Ion Inertial Fusion (HIF) requires an accelerator that can deliver beams to ignite an inertial fusion target



...or perform High-Energy Density Physics (HEDP) studies.

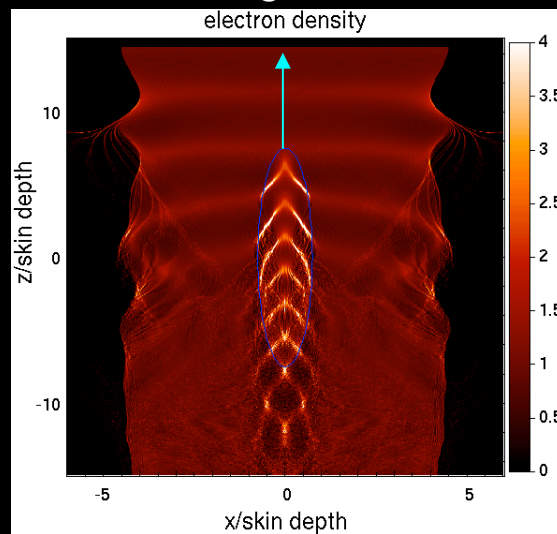
Simulation goal - predictive capability for HIFS

End-to-End 3-D self-consistent time-dependent simulations of beam, electrons and gas with self-field + external field (dipole, quadrupole, ...).

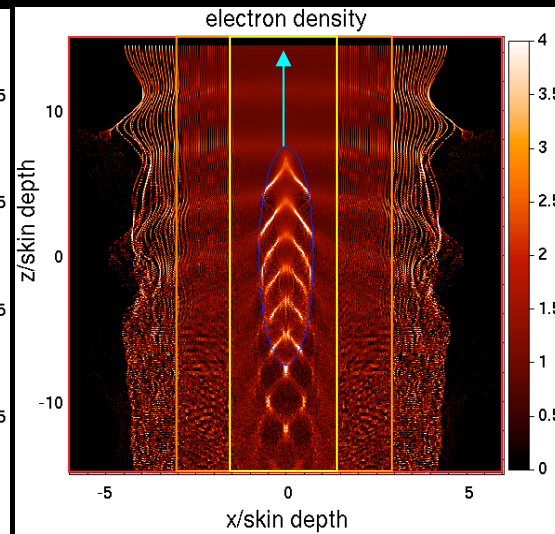


2 levels of mesh refinement (MR)

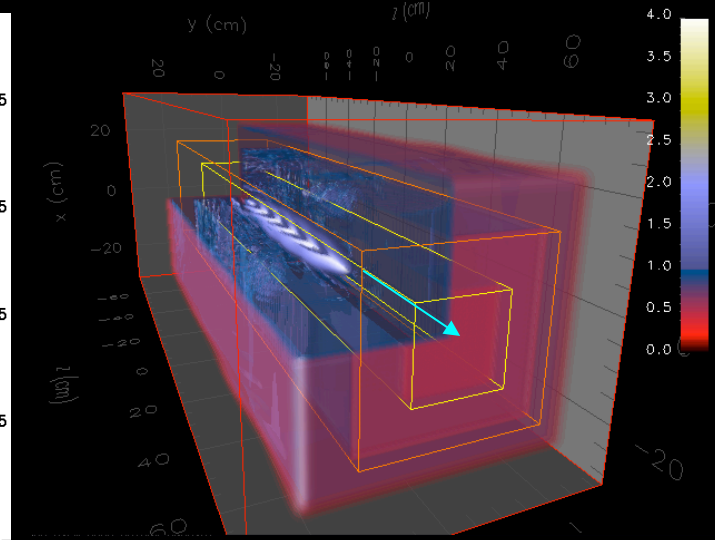
2-D high resolution



2-D low resolution + MR



3-D



These simulations used the same time steps for all refinement levels.

The implementation of separate time steps for each refinement level is underway.

Our principal goals, and activities in support of those goals, over the next five years are to:

(1) Optimize use of NDCX-II for planned target experiments

With Warp, simulate beams from source to target, in full kinetic detail, including EM effects in first-principles modeling of beam neutralization by plasma.

Use output from an ensemble of runs as input to target simulations using ALE-AMR and other codes.

(2) Develop enhanced versions of NDCX-II, and define a next-step facility

Much of the work will involve iterative optimization employing Warp runs that assume ideal beam neutralization downstream of the accelerator. At present, optimization is achieved by running ensembles, since the current simulations use too few particles for gradient-based optimizers; we hope the new computer resources will enable us to use such methods.

(3) Carry out detailed target simulations in the Warm Dense Matter regime using the ALE-AMR code, including surface tension effects, liquid-vapor coexistence, and accurate models of both the driving beam and the target geometry.

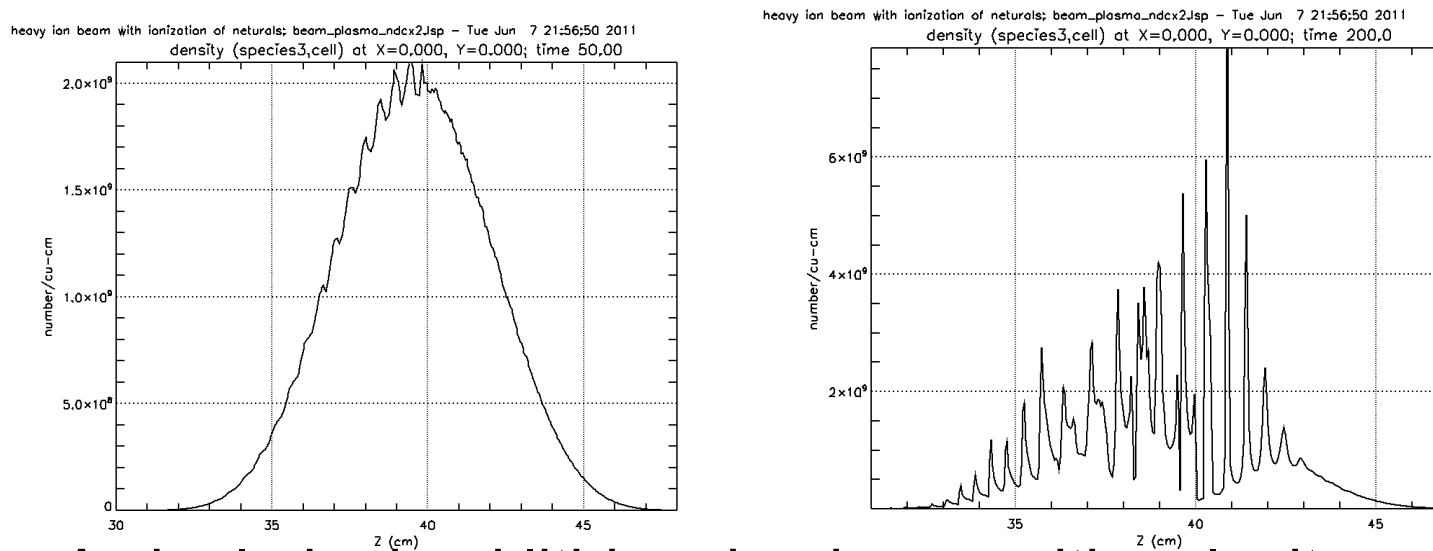
For this we will need to make multiple runs (so as to capture shot-to-shot variations), and to both develop and employ synthetic diagnostics (so as to enable direct comparison with experiments). The new science that will be revealed is the physics of the transition from the liquid to vapor state of a volumetrically superheated material, where droplets are formed, and where the physics of phase transitions, surface tension and hydrodynamics all are playing significant roles in the dynamics. These simulations will enable calculations of equation of state and other material properties, and will be of interest in their own right for their illumination of the science of droplet formation.

(4) Carry out detailed target simulations of key elements of IFE target physics using the ALE-AMR code.

This will require some further code development, TBD. At present there is no radiation model, but one might be added.

Particle-in-cell simulations reveal that two-stream instability can develop for NDCX-II parameters

Beam longitudinal density profile along the beam axis after propagation in plasma for 0.5 m (left) , and 2m (right) .

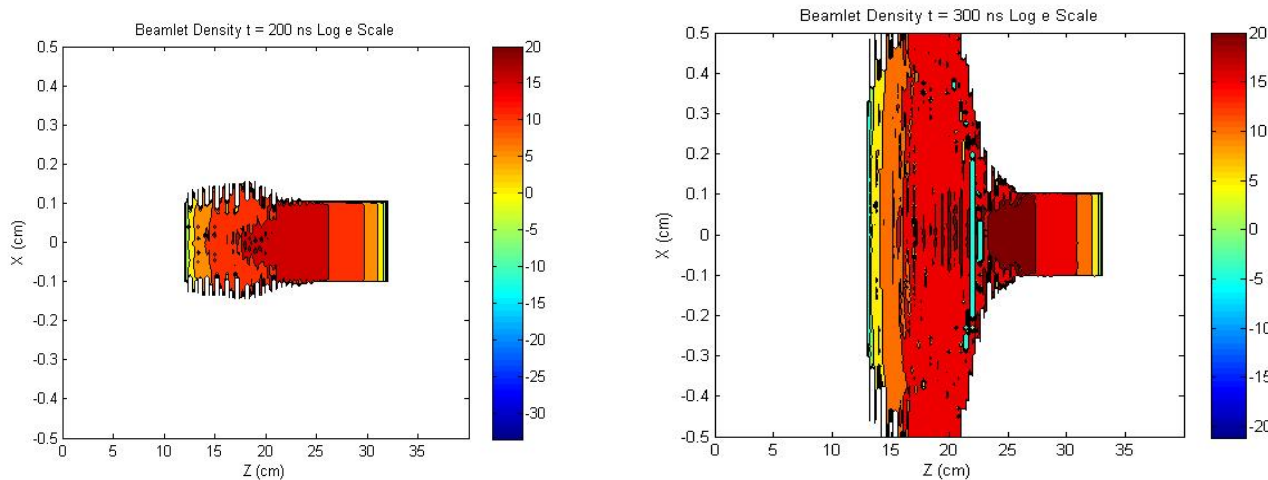


A singly-ionized lithium ion beam with velocity $v_b = c/30$ propagates through a neutralizing singly ionized background carbon plasma with density $n_p = 0.55 \times 10^{11} \text{cm}^{-3}$. Initial beam density is $n_b = 2 \times 10^9 \text{cm}^{-3}$, the beam radius is $r_b = 1.4 \text{cm}$.

Edward A. Startsev, Igor Kaganovich, and Ronald C. Davidson, "Nonlinear effects of beam-plasma instabilities on neutralized propagation of intense ion beams in background plasma", Proceedings of IFSA 2011, Bordeaux. 44

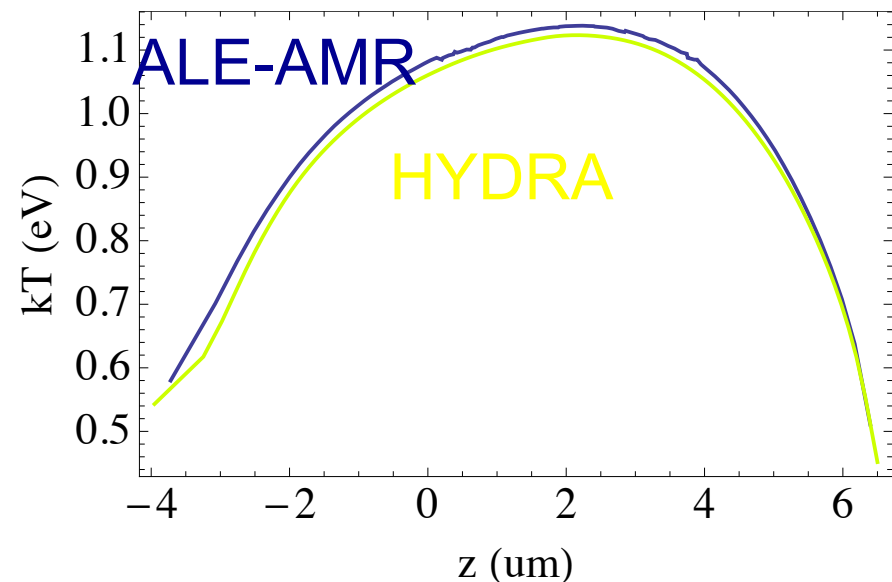
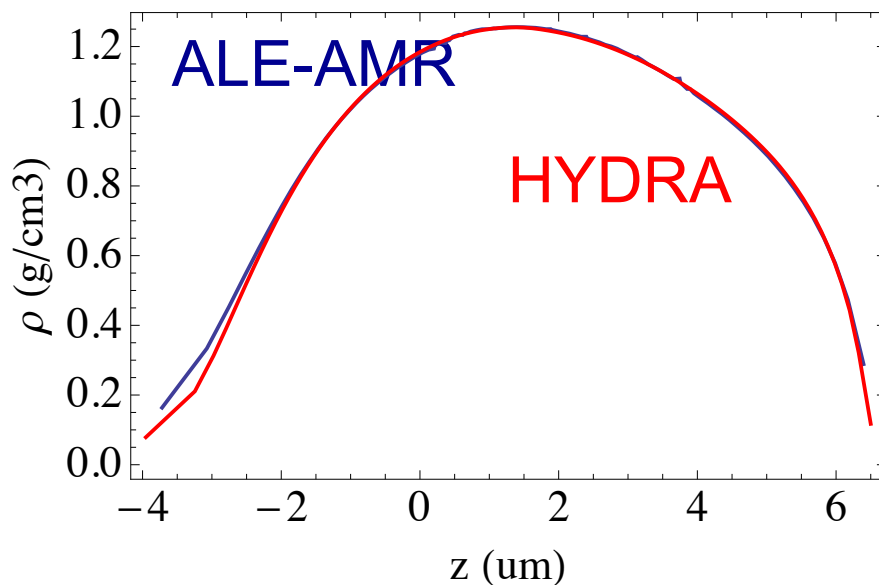
The two-stream instability does not break up NDCX-II beam but can be observed on a beamlet of much smaller radius

Color plot of beamlet density profile after propagation in plasma for 2 m (left) and 3m (right).



A singly-ionized lithium ion beam with velocity $v_b = c/30$ propagates through a neutralizing singly ionized background carbon plasma with density $n_p = 0.55 \times 10^{11} \text{cm}^{-3}$. Initial beam density is $n_b = 2 \times 10^9 \text{cm}^{-3}$, the beam radius is $r_b = 0.1 \text{cm}$.

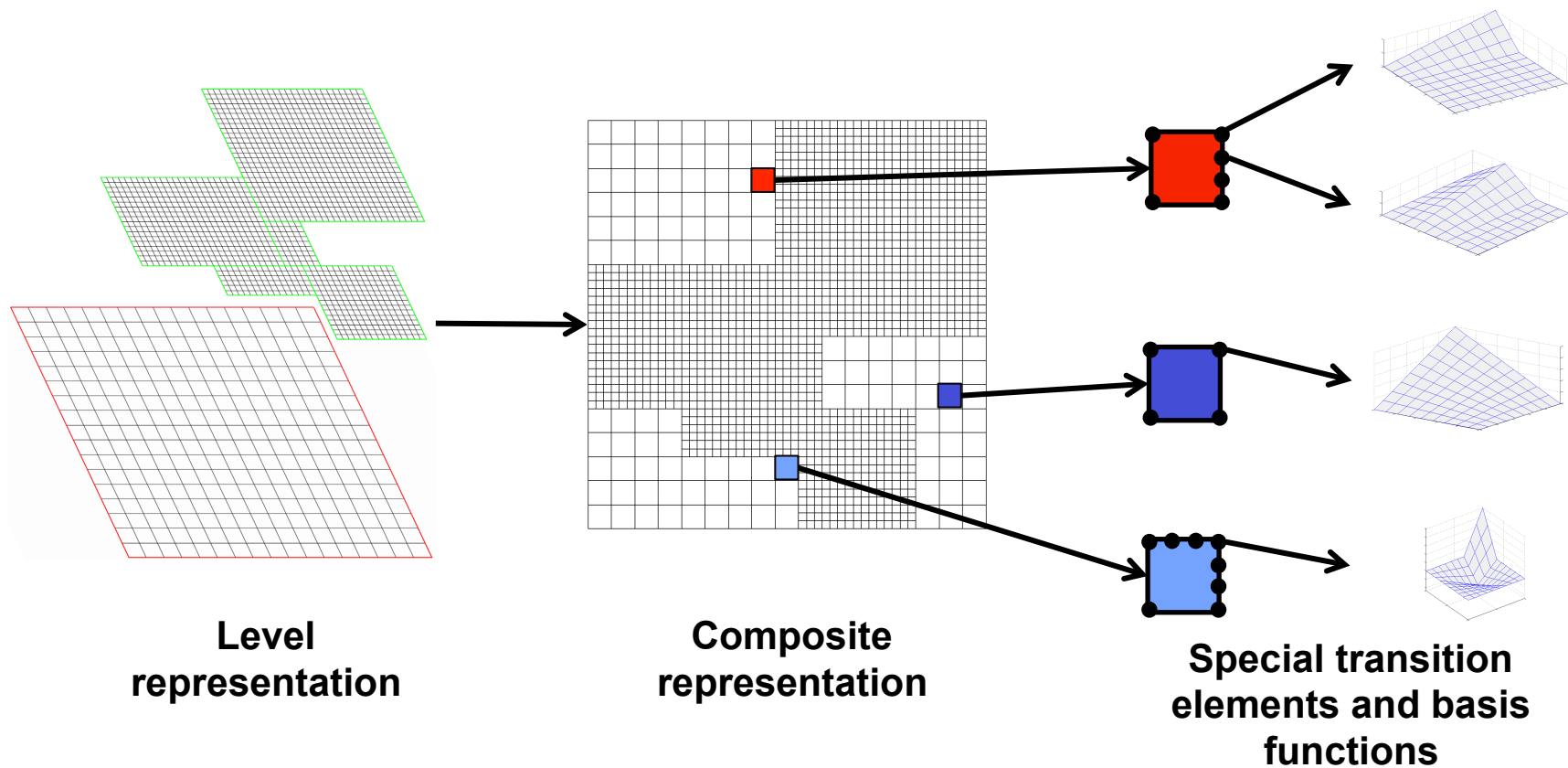
Ion beam deposition and hydrodynamics in ALE-AMR have been benchmarked against the Hydra code



Density and temperature profiles at the completion of the 1 ns, 2.8 MeV, Li ion heating pulse along the radial center of an Al foil. Fluence of 20 J/cm².

The diffusion equations are solved using the Finite Element Approach (FEM)

- We map the level representation to an equivalent composite mesh
- Special nodal basis functions are constructed to handle the C-F interface



ALE-AMR is Portable and Open Source

- C++, Fortran, Python, and some other languages
- Built with freely available libraries
 - Boost, Tvmet, GSL, CppUnit
 - SAMRAI, VisIt
 - MPICH
 - Emacs, Subversion
 - Python, SWIG, Wild Magic
- Runs on Linux
 - CHAOS at Livermore Computing
 - Cray Linux Environment at NERSC
 - SUSE at UCLA
 - Ubuntu on PC

